BOREAS An international journal of Quaternary research

Lateglacial and Holocene chronology of climate-driven postglacial landscape evolution in northeast Greenland

JULIA GARCIA-OTEYZA, MARC OLIVA, DAVID PALACIOS, JOSE MARIA FERNÁNDEZ-FERNÁNDEZ, IRENE SCHIMMELPFENNIG, MARCELO FERNANDES, SANTIAGO GIRALT, DERMOT ANTONIADES AND VINCENT JOMELLI

BOREAS

Garcia-Oteyza, J., Oliva, M., Palacios, D., Fernández-Fernández, J. M., Schimmelpfennig, I., Fernandes, M., Giralt, S., Antoniades, D. & Jomelli, V.: Lateglacial and Holocene chronology of climate-driven postglacial landscape evolution in northeast Greenland. *Boreas*. https://doi.org/10.1111/bor.12683. ISSN 0300-9483.

The Greenland Ice Sheet is highly sensitive to climate change, leading to significant retreat along its edges. This rapid ice loss contributes to rising sea levels and impacts the Earth's climate stability. Understanding the extent of recent glacier retreat is crucial in order to determine if it is unprecedented or within ranges of natural variability. Palaeoenvironmental studies aim to identify past glacial phases and landscape changes using advanced dating methods such as cosmic ray exposure (CRE) dating. In NE Greenland, CRE dating has helped establish the timing of glacial oscillations, yet a comprehensive understanding of glacial fluctuations during specific periods still needs to be developed. This study aims to chronologically constrain the postglacial landscape evolution of two NE Greenland valleys from the Young Sund–Tyrolerfjord area (74°N, 20–25°E) from the onset of deglaciation and throughout the Holocene to better understand glacial and postglacial changes. The chronological framework relies on 27 ^{10}Be cosmic-ray exposure ages that constrain our interpretation of the geomorphological features in both valleys. Inconsistencies were observed in the ages dataset, highlighting potential bias associated with nuclide inheritance and post-glacial dynamics. Despite limitations, the CRE results confirm the general pattern observed in NE Greenland: (i) major deglaciation and disconnection of glaciers from the main glacial systems during the Lateglacial and Early Holocene with a rapid but not homogeneous deglaciation within the range from ~14.3 to 11.9 ka; (ii) no evidence of glacial activity during the Middle Holocene, probably associated with the withdrawn position of the ice masses' fronts; and (iii) glacier expansion during the Late Holocene, with a Little Ice Age advance as the last significant period of glacial regrowth.

Julia Garcia-Oteyza (juliagarciadeoteyza@ub.edu) and Marc Oliva, Department of Geography, Universitat de Barcelona, Montalegre 6, 08001 Barcelona, Catalonia, Spain; David Palacios and Jose Maria Fernández-Fernández, Department of Geography, Universidad Complutense de Madrid, Calle del Profesor Aranguren, s/n. Facultad de GeografÍa e Historia, Ciudad Universitaria, 28040 Madrid, Spain; Irene Schimmelpfennig and Vincent Jomelli, Aix-Marseille Université, CNRS, IRD, INRAE, Coll. France, UM 34 CEREGE, Aix-en-Provence, France; Marcelo Fernandes, Centre of Geographical Studies, Institute of Geography and Spatial Planning, Universidade de Lisboa, Rua Branca Edmée Marques, 1600-276 Lisboa, Portugal; Santiago Giralt, Geosciences Barcelona (GEO3BCN), Carrer de Lluís Solé i Sabarís, s/n, Les Corts, 08028 Barcelona, Spain; Dermot Antoniades, Département de Géographie, Université Laval, Pavillon Abitibi-Price, 2405 Rue de la Terrasse, Québec, QC, G1V 0A6, Canada; *received 6th January 2024, accepted 21st October 2024.*

The Greenland Ice Sheet (GrIS), a tipping component of Earth's climate system (Lenton *et al*. 2008), is responding rapidly to present-day climate warming, with major retreat along most of its margins (Vasskog *et al*. 2015). Glaciers and ice caps peripheral to the main GrIS comprise a small area of Greenland's ice cover (~5%) but they contribute markedly to sea-level rise (Bjørk *et al*. 2018), currently comprising 11% of the ice loss associated with Greenland's recent sea-level rise contribution (Khan *et al*. 2022). Despite its importance, quantifying their changes and variability over multi-decadal timescales has been challenging owing to the lack of long-term data (Bjørk *et al*. 2018). This lack of data has also affected the interaction between palaeodata and past projection models of the ice-sheet extent, because although it has improved in recent years, data for mapping and dating the deglacial evolution of the GrIS land margin are scarce (Leger *et al*. 2023). This data void is most evident in the study of the evolution of Greenland's peripheral glaciers and ice caps during the Lateglacial and Holocene, since the knowledge is relatively limited and their glacial margin fluctuations still need to be better constrained (Biette *et al*. 2020). During the Early Holocene, extensive deglaciation led to the individualization of the currently peripheral glaciers from the GrIS (Håkansson *et al*. 2007, 2009, 2011; Kelly *et al*. 2008; Larsen *et al*. 2018; Skov *et al*. 2020; Axford *et al*. 2021; Garcia-Oteyza *et al*. 2022). Therefore, it is important to connect the glacial oscillations of the GrIS with the glacial history of the peripheral glaciers. GrIS melting is currently the main contributor to sea-level rise (10.8±0.9 mm between 1992 and 2018; IMBIE Team 2020); this contribution may further accelerate in the coming decades as the GrIS is in imbalance with the current climate and there is a temporal delay in the ice sheet's response (King *et al*. 2020). The loss of glacial ice has major implications for ocean currents, sea ice and surface radiative balance that affect the stability of Earth's climate system (Meredith *et al*. 2019).

DOI 10.1111/bor.12683

Recent advances in absolute dating have refined the chronologies of past glacial dynamics, with particular success in the use of cosmic ray exposure (CRE) dating of glacial landforms (Gosse & Klein 2014; Balco 2019). In NE Greenland, the focus of this study, CRE dating has been increasingly used over the last several years to frame the timing of glacial oscillations (Håkansson *et al.* 2007, 2009, 2011; Kelly & Lowell 2008; Lowell *et al.* 2013; Levy *et al.* 2014; Larsen *et al.* 2018; Skov *et al.* 2020; Biette *et al.* 2020; Garcia-Oteyza *et al.* 2022, 2023a). Despite this, our knowledge of the temporal and spatial deglaciation patterns and postglacial landscape evolution across NE Greenland for certain periods should be improved, particularly during Termination-1 (T-1; ~19–20 to 11.7 ka) and the Early Holocene (~11.7–8.2 ka), when most of the currently ice-free areas became deglaciated (e.g. Håkansson *et al.* 2007, 2009, 2011; Kelly *et al.* 2008; Larsen *et al.* 2018; Skov *et al.* 2020; Garcia-Oteyza *et al.* 2022). Since T-1, glaciers have recorded only minor advances and retreats, with the Little Ice Age (LIA; ~0.6–0.2 ka BP) being the most recent period with a documented widespread glacial expansion in NE Greenland (Biette *et al.* 2020; Jomelli *et al.* 2022; Garcia-Oteyza *et al.* 2023a).

In some cases, the application of CRE dating in NE Greenland is strongly influenced by the occurrence of nuclide inheritance and postglacial environmental dynamics, including paraglacial readjustment or mass movements following glacier retreat. Greenlandic areas affected/covered by non-erosive cold-based ice, frozen to the bed, in many parts of Greenland (Bierman *et al.* 2014; Paxman *et al.* 2024) lead to the preservation and co-existence of the glacial record from several glaciations. Hence, this can impede robust dating of the glacial record from the last glacial cycle and subsequent deglaciation (Skov *et al.* 2020). In addition, some studies have also highlighted the impact of postglacial dynamics on the conservation of the glacial signal and interpretation of the geomorphological significance of the dated samples (Garcia-Oteyza *et al.* 2022). Therefore, special care needs to be taken when taking CRE dating samples and interpreting postglacial landscape evolution based on their results.

The objective of this study is to chronologically constrain the glacial and postglacial landscape evolution of two valleys from two peripheral ice caps at the Young Sund–Tyrolerfjord area, from the Lateglacial and throughout the Holocene, to shed light on glacial responses to climate variability in the region and to assess the environmental transformation following deglaciation. To this end, we had the following specific objectives: (i) to identify and differentiate landforms generated by glacial oscillations and by paraglacial processes; (ii) to identify the main phases of glacial expansion and retreat, as well as the major postglacial environmental processes reshaping the glacial landscape; (iii) to compare spatio-temporal patterns of glacial and postglacial landscape evolution in these valleys with those patterns detected in other regions across NE Greenland in other studies; and (iv) to identify the value of CRE dating in an environment of cold-based glaciers and intense paraglacial and periglacial processes accompanying deglaciation and rapid temperature increases.

Regional setting

This study focuses on two deglaciated U-shaped valleys located in the NE Greenland National Park: Olsen Valley, in the interior of the Wollaston Forland Peninsula; and Dolomit Valley, on the northern coast of Clavering Island (Fig. 1).

The Olsen Valley extends over ~10 km NW–SE from the shoreline of the Store Sødal Lake to the front of the SE Outlet Glacier (SEOG) of the A.P. Olsen Land Ice Cap (Fig. 2). This is a predominantly cold-based ice cap (Behm *et al.* 2020), with its front located ~35 km inland from the Zackenberg Research Station (Fig. 1). Two deglaciated tributary valleys descending from the NE and SW sides merge with the main valley floor at the middle part of the Olsen Valley. The surrounding flat-topped summits around the Olsen Valley rise on either side to elevations between 800 and 1200 m above sea level (a.s.l.) and connect with steep hillsides (up to 20–35°) descending into the valley. Quaternary sediments cover the valley floor and the slopes, while metamorphic rocks (relatively homogeneous Paleoproterozoic orthogneiss) are exposed on the upper slope sections (Koch & Haller 1971). A braided river system fed by SEOG meltwater and other streams descending from the surrounding mountains occupies the valley floor and flows into the Store Sødal Lake. The Olsen Valley and the river that flows 38 km to the Zackenberg delta is repeatedly affected by glacial lake outburst floods (GLOFs). These abrupt events originate at the ice-dammed lake impounded by the SEOG that dams an adjacent ice-free side valley; here, water accumulates and forms a lake, which is regularly drained over a quasi-annual cycle monitored since the first known GLOF in 2005 (Behm *et al.* 2020). These events have a strong influence on environmental dynamics at the catchment scale (Kroon *et al.* 2017), with occasional megaflood characteristics (Behm *et al.* 2020).

The Dolomit Valley stretches ~5 km NE–SW between the coast at the Young Sound fjord and the Dolomit Glacier front (Fig. 3). The valley includes only one tributary in its upper part that is still partially occupied by a small alpine glacier descending from the mountain plateaus distributed at elevations of 1000–1200 m a.s.l. The hillsides descending from these flat-topped summits are moderately sloped (15–25°). A braided river with a high sediment load flows along the valley floor, and has created a delta in contact with the Young Sound fjord (Kroon *et al.* 2017). Dolomit Valley is crossed by a normal fault as this valley

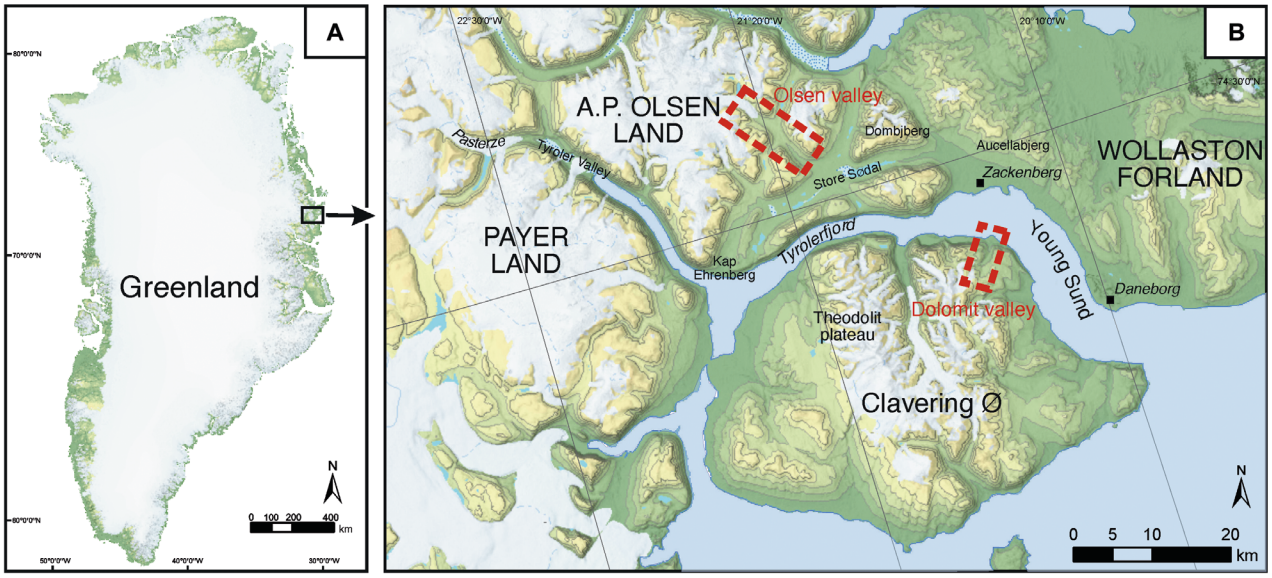

Fig. 1. A. Location of the study area within Greenland. B. Detail of the study region with the study areas.

constitutes the boundary between the central and eastern geological sections of Clavering Island (Koch & Haller 1971). The western slopes consist of metasediments, gneiss and granite formations of Caledonian Crystalline complexes, whereas the eastern slopes are formed by Jurassic and Cretaceous sedimentary rocks (mudstones, sandstones and carbonates; Grønnow *et al.* 2009). As a result, thick re-deposited Quaternary sediments affected by active hillside processes cover the middle and lower sections of the slopes.

The regional climate regime is defined as a High Arctic polar tundra climate (Kottek *et al.* 2006). The nearby Zackenberg Research Station records an average annual air temperature of −9.0 °C (1996–2015), with monthly mean temperatures ranging from −19.8 °C in February to 6.3 °C in July (Højlund Pedersen 2017). The mean annual precipitation is 367 mm, mainly falling as snow (Hansen *et al.* 2008). The area is snow-covered most of the year, generally from September to the end of May, although with a large interannual variability (Hinkler *et al.* 2008; López-Blanco *et al.* 2020). Permafrost controls present day geomorphological processes in the region; it is continuous and shows thicknesses up to 200–400 m, as observed in the nearby Zackenberg Valley (Christiansen *et al.* 2008; Christoffersen, Amsinck *et al.* 2008; Christoffersen, Jacobs *et al.* 2008; Hansen *et al.* 2008). The vegetation in this area is predominantly composed of dwarf shrub heaths, with diversity and size diminishing as elevation increases. Below 200 m a.s.l. small shrubs, fell fields and grasses prevail (CAVM Team in 2003), whereas above 600 m a.s.l. vegetation becomes very scarce (Buus-Hinkler *et al.* 2006; Elberling *et al.* 2008).

Methodology

In this study, we integrated geomorphological and geochronological (CRE ^{10}Be dating) approaches. The fieldwork was conducted in early September 2019, when the snow-free environment enabled a precise identification of geomorphological features and the collection of samples for CRE dating.

Geomorphological mapping

Prior to fieldwork, we mapped geomorphic landforms based on satellite imagery. This preliminary map underwent validation through *in-situ* observations and also incorporated newly identified landforms. The final geomorphological maps were delineated within the ArcMap 10.8 work environment, based on WorldView-2 orthorectified panchromatic satellite images with imagery (0.5-m resolution) from 2018 for Olsen Valley and WorldView-3 imagery (0.3-m resolution) from 2019 for Dolomit Valley in conjunction with the shaded relief elevation raster derived from the Arctic DEM digital elevation model (2-m resolution) (Porter *et al.* 2018).

Sample collection strategy

We collected 15 samples from the Olsen Valley and 12 more from the Dolomit Valley for ^{10}Be CRE dating. Each sample consisted of ∼1 kg of the uppermost rock layer (maximum thickness of ≤5 cm) using a hammer and chisel. We refrained from sampling at corners, edges and steep faces (>20°) to optimize the reception of cosmic ray flux. The selection of boulders for sampling is contingent upon their deep anchoring in the ground to

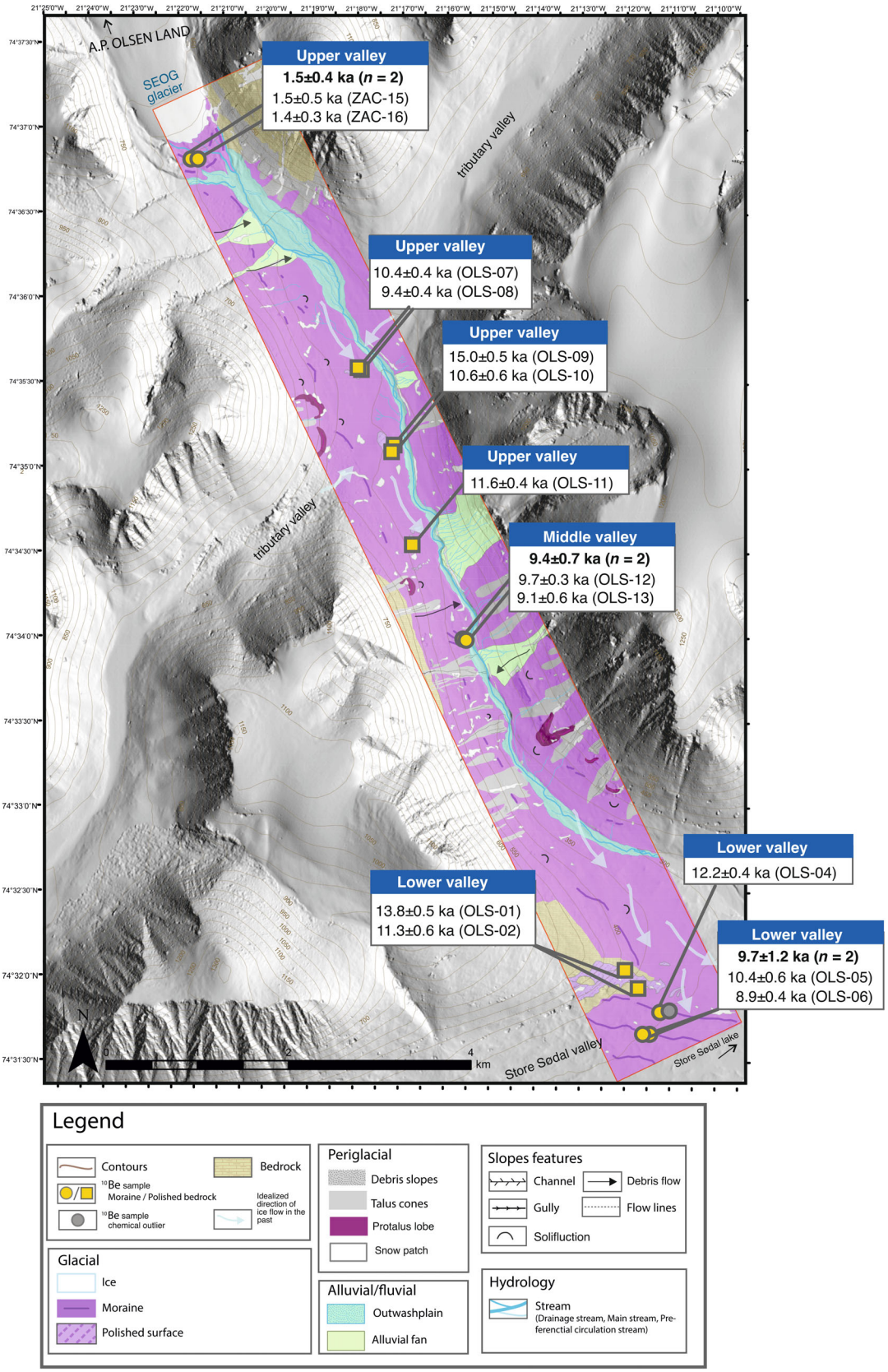

Fig. 2. Olsen Valley geomorphological map including the main landforms together with the cosmic ray exposure (CRE) results shown in Tables 1 and 2.

ensure stability and minimize the risk of boulder collapse. These boulders are positioned on moraine crests, protruding in a manner that makes it unlikely that they have been covered by sediments since their deposition. For the polished bedrock samples the necessary observations were made to avoid pre-exposure memory problems (insufficient glacial erosion). Concurrently, we documented key details such as the geomorphological setting, geographic coordinates, elevation and measurements necessary for subsequent geometric adjustments to account for topographic shielding effects from the surrounding relief. A comprehensive compilation of field data and sample attributes is presented in Table 1.

CRE laboratory procedures and age calculation

Sample crushing and sieving (0.25–1-mm fraction) were carried out at the Laboratory of Physical Geography in the Universidad Complutense de Madrid, Spain. Subsequent physical and chemical procedures were conducted at the Laboratoire National des Nucleides Cosmogéniques (LN_2C) of the Centre Européen de Recherche et d'Enseignement des Géosciences de l'Environnement (CEREGE, Aix-en Provence, France). Laboratory procedures followed the same protocols as outlined in Garcia-Oteyza *et al.* (2022).

$^{10}Be/^{9}Be$ ratio measurements were performed on the BeO targets at the French 5 MV Accélérateur pour les Sciences de la Terre, Environnement et Risques (ASTER) national facility at CEREGE, with identical calibrations and standards to those described in Garcia-Oteyza *et al.* (2022). Owing to problems in the separation of quartz and the impossibility of continuing with the treatment, one sample (DOL-05) was discarded. Two samples exhibited invalid AMS measurements (DOL-03 and DOL-06) and three others showed low current values (DOL-02, DOL-09 and OLS-03). Consequently, these samples were identified as chemical outliers and were thus excluded from subsequent calculations and discussion. A comprehensive record with all analytical data is provided in Table 2.

Exposure ages were determined through the CRONUS-Earth online calculator, version 3.0 (Balco *et al.* 2008; https://hess.ess.washington.edu/), chosing the the Arctic-wide sea level/high-latitude ^{10}Be production rate (4.04 ± 0.15 atoms g^{-1} a^{-1}) (Young *et al.* 2013b) and the 'Lm' (Lal/Stone) time-dependent scaling model (Lal 1991; Stone 2000). A 2.7 g cm^{-3} density was assumed for all samples. No corrections for erosion or snow shielding were considered in accordance with earlier studies on the area (Garcia-Oteyza *et al.* 2022, 2023a). The partial shielding effect of the surrounding topography was accounted for with the 'Topographic Shielding Calculator v.2' (http://stoneage.ice-d.org/math/skyline/skyline_in.html) for all sampling sites (see Table 2 for details). Exposure ages are given in Table 2 with their internal (only analytical) and external uncertainties (including production rate uncertainty). In the text and the figures, ages are given with their internal uncertainties unless otherwise stated. The mean ages shown were calculated arithmetically, and their uncertainties include the standard deviations of the single ages and the squared production rate uncertainties.

Results

The spatial distribution and typology of geomorphological features distributed in both valleys provide insights into the glacial and postglacial landscape evolution of the area over the last several millennia (Figs 2, 3). The chronological framework of the geomorphic evolution in these two valleys is constrained by the 27 ^{10}Be CRE ages obtained from glacial and slope records (Table 2).

Geomorphological setting and exposure ages

Both valleys are U-shaped, and are almost entirely deglaciated, preserving geomorphic evidence of past periods with larger ice masses. Some glacial landforms around the working areas have been affected by paraglacial slope processes and special caution must therefore be taken when reconstructing the geomorphological evolution (even if these were not dated landforms). Based on the distribution of the major glacial landforms, we can track the past environmental dynamics occurring in the region since the onset of the deglaciation of the valleys. Chronological data and geographical characteristics of the samples are presented in Figs 2 and 3 together with photographs of the study area showing the different geomorphological units (Fig. 4). Here, we present the CRE dating results in the two valleys from the lower sections up to the ice fronts.

Olsen Valley. – The Olsen Valley only includes one major ice tongue descending 6.5 km from the A.P. Olsen Ice Cap (SEOG glacier) forming two well-defined frontal moraine ridges. Towards the middle of the valley, two ice-free tributary valleys merge with the Olsen Valley from its NE and SW edges (Fig. 2). Above ~550 m a.s.l. the metamorphic bedrock of this area remains exposed on relatively flat and mostly deglaciated mountain plateaus. Discontinuous till with some minor moraine ridges covers the steep mountain slopes, with small and frequent exposures of polished bedrock surfaces across the slope's lowest parts. This dynamic geomorphological setting favoured the occurrence of very active periglacial processes on the slopes that triggered the development of protalus lobes, talus cones, debris flows and alluvial fans, which, in turn, impeded the preservation of well-preserved datable glacial records as most were largely covered or eroded by postglacial slope processes (Fig. 2). An outwash plain fed by glacial meltwater extends over much of the valley floor, and narrows downslope where it

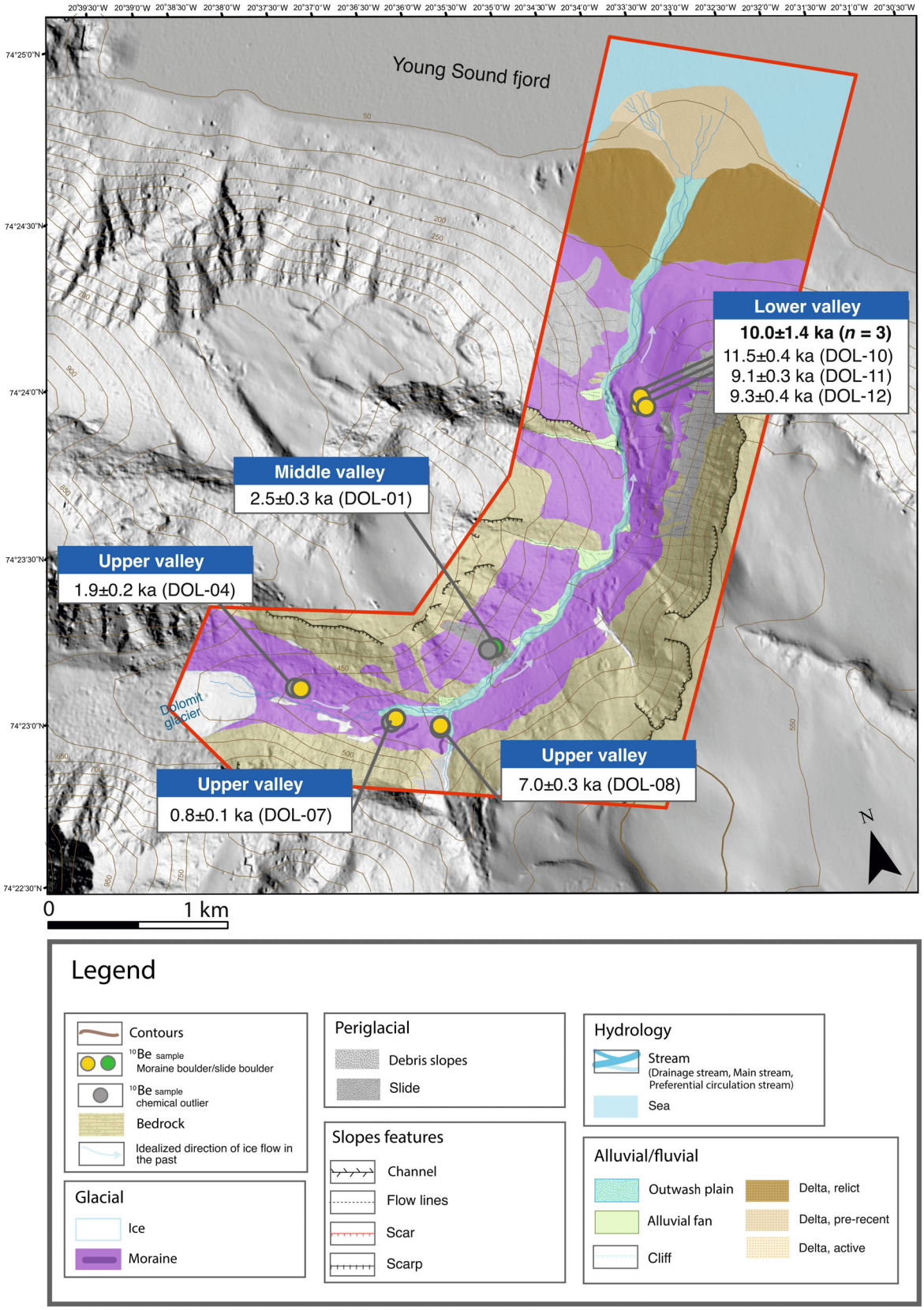

Fig. 3. Dolomit Valley geomorphological map including the main landforms together with the cosmic ray exposure (CRE) results shown in Tables 1 and 2.

Table 1. Sample locations, topographic shielding factors and sample thicknesses. Chemical outlier sample information is shown in italics.

Sample ID	Landform	Latitude (DD)	Longitude (DD)	Elevation (m a.s.l.)	Topographic shielding factor (dimensionless)	Thickness (cm)
Olsen Valley						
OLS-01	Polished surface	74.53515	−21.196561	389	0.9932	2.5
OLS-02	Polished surface	74.534466	−21.192555	334	0.9894	2.5
OLS-03 (L:0.9, l:0.6, H:0.5, h:0.3)	*Lateral moraine*	*74.530252*	*−21.190141*	*251*	*0.9971*	*0.5*
OLS-04 (L:0.8, l:0.7, H:0.5, h:0.4)	Lateral moraine	74.526673	−21.18916	242	0.9972	1.5
OLS-05 (L:1.3, l:1, H:0.7, h:0.4)	Lateral moraine	74.526646	−21.174735	231	0.9974	1.5
OLS-06 (L:1.2, l:1.1, H:0.8, h:0.5)	Lateral moraine	74.526578	−21.174642	231	0.9981	1.5
OLS-07	Polished surface	74.592999	−21.302957	263	0.9937	1.5
OLS-08	Polished surface	74.592188	−21.301233	263	0.9937	1.5
OLS-09	Polished surface	74.58642	−21.290792	231	0.9934	2.5
OLS-10	Polished surface	74.585605	−21.289947	228	0.9934	2.5
OLS-11	Polished surface	74.575724	−21.28058	293	0.9925	2.5
OLS-12 (L:2.2, l:1.3, H:1.2, h:0.6)	Lateral moraine	74.566978	−21 261 636	183	0.9903	1.5
OLS-13 (L:1.8, l:1.5, H:1, h:0.3)	Lateral moraine	74.566978	−21.261823	183	0.9903	1.5
ZAC-15	Frontal moraine	74.56523	−21.53018	516	0.9788	2.6
ZAC-16	Frontal moraine	74.5645	−21.52769	556	0.9692	3.8
Dolomit Valley						
DOL-01 (L:1, l:1, H:0.8, h:0.5)	Slide boulder	74.380382	−20.615017	336	0.9942	1.5
DOL-02 (L:1.3, l:1, H:0.7, h:0.4)	*Slide boulder*	*74.380576*	*−20.614789*	*335*	*0.9937*	*2.5*
DOL-03 (L:3.5, l:1.5, H:1.5, h:0.8)	*Lateral moraine*	*74.382262*	*−20.658827*	*500*	0.9873	*0.5*
DOL-04 (L:2.2, l:1.5, H:1.5, h:1.1)	Lateral moraine	74.382227	−20.65788	502	0.9873	0.5
DOL-05(L:2.7, l:2.1, H:1.1, h:0.9)	*Lateral moraine*	*74.377432*	*−20.638129*	*417*	*0.9927*	*1.5*
DOL-06 (L:1.2, l:1.2, H:0.5, h:0.3)	*Lateral moraine*	*74.377492*	*−20.638035*	*418*	*0.9927*	*0.5*
DOL-07 (L:1, l:0.8, H:0.7, h:0.4)	Lateral moraine	74.377384	−20.640582	424	0.9924	0.5
DOL-08 (L:1.3, l:1, H:0.8, h:0.4)	Lateral moraine	74.37714	−20.634161	395	0.9855	2.5
DOL-09 (L:1, l:1, H:1, h:0.6)	*Lateral moraine*	*74.377078*	*−20.634958*	*405*	*0.9855*	*2.5*
DOL-10 (L:2, l:1.3, H:1.3, h:0.7)	Lateral moraine	74.390437	−20.576733	244	0.9882	2.5
DOL-11 (L:2, l:1.5, H:1.1, h:0.8)	Lateral moraine	74.390499	−20.577294	245	0.9865	1.5
DOL-12 (L:1.3, l:1.1, H:1.1, h:0.9)	Lateral moraine	74.390598	−20.577354	245	0.9882	2.5

is gradually by a braided river system with traces of erosion in the river banks triggered by GLOF events that also disrupted glacial sedimentary records existing on the valley floor. The CRE dating results (a total of 15 samples) of the Olsen Valley show ages between the last stages of T-1 and the Early Holocene and can be explained within the three different sectors of this valley that were observed:

- *Lower valley.* The moraines at the confluence with the Store Sødal valley are indicative that the area must have been occupied by a single glacial tongue formed by the coalescence of the SEOG glacier and the Store Sødal valley glacier descending from the ice sheet (Fig. 2). In this large flat area, a lobate piedmont glacier generated multiple moraine ridges with abundant till dispersed across the valley bottom. Recurrent high-energy GLOFs cut the lowest part of this moraine complex and eroded the flanks of the valley floor up to the glacial front. In the highest part of this moraine complex, at the entrance of the valley, there is a polished surface partially covered by till. Considering the limited availability of well-preserved glacial records and the intensity of alluvial and slope processes in the area, we collected six samples from this area distributed at different elevations: two from polished and striated bedrock surfaces at ∼390 and ∼330 m a.s.l., yielding exposure ages of 13.8±0.5 ka (OLS-01) and 11.6±0.6 ka (OLS-02) respectively; and three from moraine ridges – one from a moraine ridge at ∼250 m a.s.l. that stands out sharply in height above the others and has great lateral continuity, extending laterally from the foot of the slope to the head of the Store Sødal lake where it has been dismantled by a large alluvial fan and returned an age of 12.2±0.4 ka (OLS-04) (Fig. 4G) and two more from the most well defined blocky moraine in the sector moraine ridge at ∼230 m a.s.l. that yielded ages of 10.4±0.4 ka (OLS-05) and 8.9±0.4 ka (OLS-6), respectively, with a mean age of 9.7±1.2 ka (n = 2).
- *Middle valley.* Towards the middle of the valley, the second frontal moraine complex is composed of three minor smoothed moraine ridges with the presence of large blocks along the higher parts. These ridges are indicative of the occurrence of glacial standstills or advances within the long-term retreat. Two samples were taken on the intermediate ridge of the complex at

Table 2. AMS analytical data and calculated exposure ages. $^{10}Be/^{9}Be$ ratios were inferred from measurements made at the ASTER AMS facility. No corrections for erosion and snow cover were made. Chemical outliers and samples rejected owing to geomorphological interpretation reasons are highlighted in italics. See Methodology and Results sections for more explanation.

Sample name	Quartz weight (g)	Mass of carrier (mg ^{9}Be)	$^{10}Be/^{9}Be$ (10^{-14})	Blank correction (%)	(^{10}Be) (10^{4} atoms g^{-1}) $\pm1\sigma$ (atoms g^{-1})	^{10}Be age (ka)[1]	Internal uncertainty (ka)	External uncertainty (ka)
Olsen Valley								
OLS-01	33.9929	0.44667	11.154±0.372	2.06	5.129±0.327	13.8	0.5	0.7
OLS-02	8.0601	0.44259	2.223±0.098	8.88	7.537±0.378	11.3	0.6	0.7
OLS-03	*23.3613*	*0.44812*	*16.144±6.105*	*1.42*	*20.399±7.825*	*30.8*	*11.9*	*12.0*
OLS-04	19.1958	0.44649	5.129±0.160	4.48	7.615±0.253	12.2	0.4	0.6
OLS-05	12.5166	0.46718	2.721±0.134	6.97	6.314±0.341	10.4	0.6	0.7
OLS-06	16.5553	0.45248	3.154±0.146	6.21	5.403±0.272	8.9	0.4	0.6
						Arithmetic mean age: 9.7±1.2 ka (n = 2)		
OLS-07	24.3783	0.36370	8.217±0.289	3.44	7.91±0.291	10.4	0.4	0.5
OLS-08	13.3286	0.44685	3.441±0.141	6.68	7.195±0.323	9.4	0.4	0.5
OLS-09	*38.9868*	*0.44428*	*15.261±0.478*	*1.48*	*11.449±0.366*	*15.0*	*0.5*	*0.7*
OLS-10	7.2783	0.40868	2.344±0.110	9.25	7.98±0.427	10.6	0.6	0.7
OLS-11	18.9395	0.43772	5.858±0.191	4.00	8.684±0.299	11.6	0.4	0.6
OLS-12	35.5021	0.44740	8.285±0.267	2.77	6.784±0.226	9.7	0.3	0.5
OLS-13	8.6230	0.45505	2.004±0.107	9.72	6.38±0.389	9.1	0.6	0.7
						Arithmetic mean age: 9.4±0.7 ka (n = 2)		
ZAC-15	15.996	0.95051	1.114±0.269	28.09	1.05±0.358	1.5	0.5	0.5
ZAC-16	21.591	0.94236	1.352±0.223	23.35	1.00±0.220	1.4	0.3	0.3
						Arithmetic mean age: 1.5±0.4 ka (n = 2)		
Dolomit Valley								
DOL-01	16.3260	0.43814	0.991±0.103	20.40	1.795±0.191	2.5	0.3	0.3
DOL-02	*7.4488*	*0.44655*	*1.839±0.241*	*10.79*	*6.571±0.972*	*11.4*	*1.7*	*1.7*
DOL-03								
DOL-04	36.3018	0.44710	1.795±0.166	12.80	1.288±0.139	1.9	0.2	0.2
DOL-05								
DOL-06								
DOL-07	30.8826	0.44788	0.755±0.087	29.66	0.515±0.093	0.8	0.1	0.2
DOL-08	16.4179	0.45605	2.45±0.105	7.93	4.187±0.201	7.0	0.3	0.4
DOL-09	*51.8427*	*0.44903*	*5.593±0.493*	*3.53*	*3.123±0.286*	*5.1*	*0.5*	*0.5*
DOL-10	28.4067	0.44821	5.763±0.193	3.43	5.868±0.205	11.5	0.4	0.6
DOL-11	38.2503	0.44658	6.288±0.224	3.57	4.731±0.177	9.1	0.3	0.5
DOL-12	31.3997	0.44734	5.302±0.196	4.33	4.829±0.189	9.3	0.4	0.5
						Arithmetic mean age: 10.0±1.4 ka (n = 3)		

Chemistry blank details[2]

Blank name	Mass of carrier (mg ^{9}Be)	$^{10}Be/^{9}Be$ (10^{-14})	(^{10}Be) (10^{4} atoms)
BK1	0.45088	0.222±0.04	6.703±1.219
BK2	0.44576	0.23±0.032	6.862±0.964
BK3	0.45242	0.196±0.028	5.921±0.832
BK4	0.96595	0.380±0.0066	6.57±0.994

[1] ^{10}Be ages assuming a density of 2.7 g cm^{-3} and a zero-erosion scenario.
[2] In parallel to the sample treatment, four blanks were prepared: BK1 (processed with samples OSL-09, DOL-07 and DOL-11), BK2 (processed with samples OSL-01, OSL-03, OSL-04, OSL-07, OSL-08, OSL-11, OSL-12, DOL-04 and DOL-12), BK-03 (processed with samples OSL-02, OSL-05, OSL-06, OSL-10, OSL-13, DOL-01, DOL-02, DOL-08 and DOL-09) and BK4 (processed with samples ZAC-15 and ZAC-16).

~180 m a.s.l, which was the best-preserved unit and that least affected by postglacial processes. These samples returned exposure ages of 9.7±0.3 ka (OLS-12) and 9.1±0.6 ka (OLS-13), with a mean age of 9.4±0.7 ka (n = 2).

- *Upper valley.* Upstream, the valley is entirely covered by till up to the glacier front. There are only few exposed sectors of polished and striated bedrock that have not been covered by postglacial sedimentary processes or affected by erosion associated with GLOF events. From this area, we collected seven samples at increasing distances from the present-day glacier front: two polished surface samples at the confluence with the two tributary valleys ~2.5 km from the glacier at ~260 m a.s.l.; two more ~3.5 km from the front at ~230 m a.s.l; and the last ~5 km from the ice limit at ~290 m a.s.l. (OLS-11). No clear datable polished surfaces were found closer to the glacier front. This sequence of samples from an exposed polished surface along the upper valley towards the glacial front returned exposure ages of 11.6±0.4 ka (OLS-11), 15.0±0.4 ka (OLS-09)

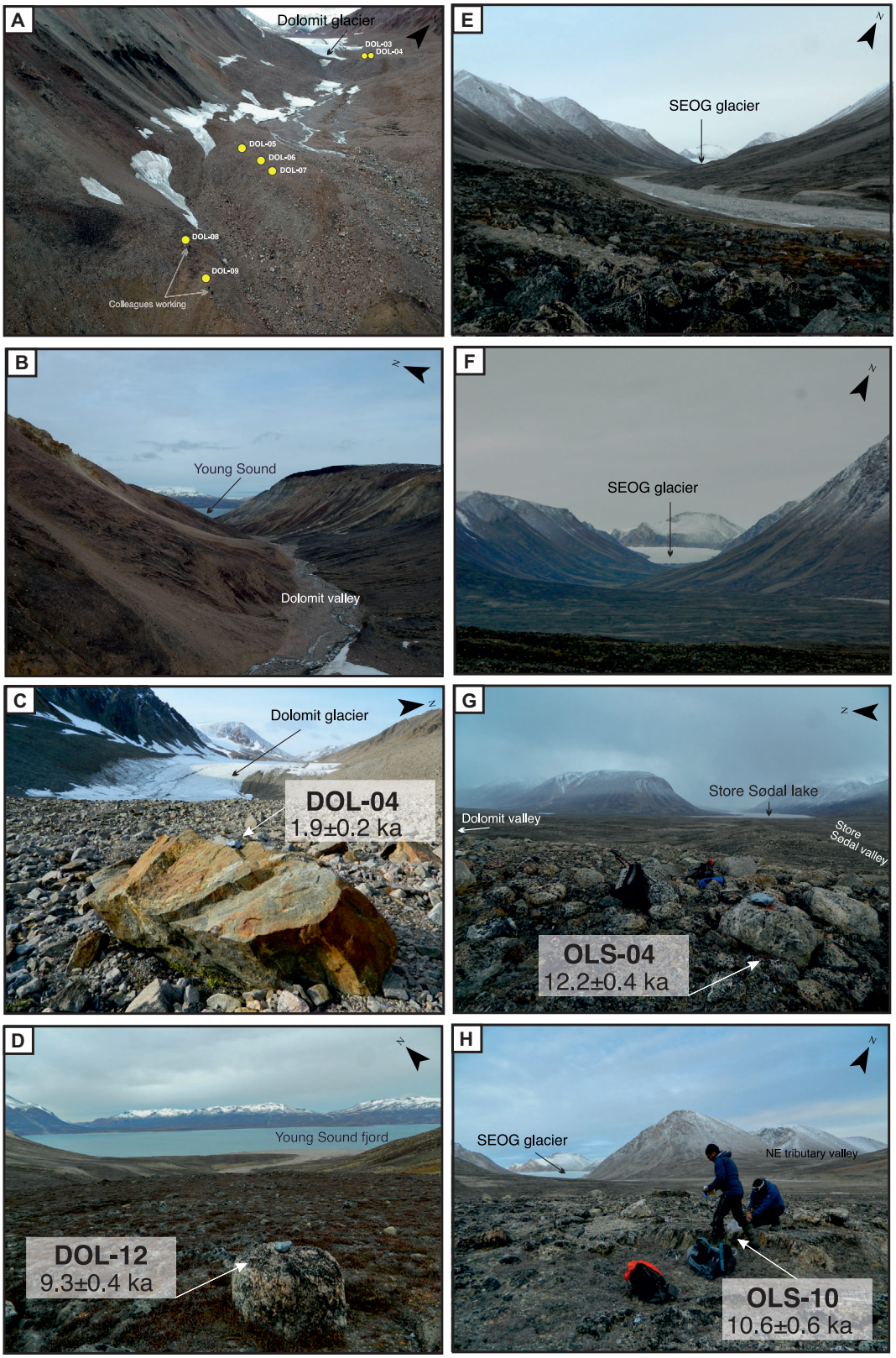

Fig. 4. Examples of the different types of sampled and dated glacial landforms. See Figs 2 and 3 for the locations of the samples shown in the photographs. A. Samples location (northwest direction view) at the Dolomit Valley. B. Northeast view of the Dolomit Valley. C. Northwest view of the Dolomit Valley. D. Northeast view of the Dolomit Valley. E and F. Northwest views of the Olsen Valley. G. East view of the Olsen Valley. H. Northwest view of the Olsen Valley.

and 10.6±0.6 ka (OLS-10) (Fig. 4D), whereas the two samples collected next to the current ice margin yielded exposure ages of 10.4±0.6 ka (OLS-07) and 9.4±0.4 ka (OLS-08). Two samples were taken from moraine boulders from the frontal moraine ridge at ~200 m from the present glacier front at ~500 m a.s.l., returning ages of 1.5±0.5 ka (ZAC-15) and 1.4±0.3 ka (ZAC-16).

Dolomit Valley. – The Dolomit Valley is mostly deglaciated, with a small mountain glacier (~3 km^2) at its head whose front is currently located ~4.5 km from the coastline. In the upper part of the valley, a single north–south deglaciated tributary merges with the valley, providing abundant sediment supply to the main river. Above ~450 m a.s.l. on the mountain plateaus, the bedrock is largely exposed, intensely weathered and affected by very active periglacial processes. The highly weatherable sedimentary rocks supplying fine loose sediments and the abundant till deposits determine the high sediment load transported by the Dolomit River to the coastal zone, forming a delta. The preservation of glacial landforms in the Dolomit Valley is largely affected by periglacial slope processes, which have altered local slope stabilities and reshaped the hillsides forming talus slopes and cones, solifluction, alluvial fans, landslides, etc. Three different sections were identified in this valley and (Fig. 3) and the age dataset (seven samples) for the Dolomit Valley is distributed as follows:

- *Lower valley.* Above the delta, there is a ~30–40 m-thick moraine ridge (NE), from where we collected three sub-angular lichenized boulder samples ~245 m a.s.l. These samples yielded ages of 11.5±0.4 ka (DOL-10), 9.1±0.3 ka (DOL-11) and 9.3±0.4 ka (DOL-12) (Fig. 4B) with a mean age of 10.0±1.4 ka (n = 3).
- *Middle valley.* On the NW side of the valley, a large landslide occurred following deglaciation. The landslide includes minor landforms, with the presence of several debris flows and very active solifluction dynamics that are indicative of intense reworking of the major slope deposit. A boulder sample was taken ~335 m a.s.l. in the most horizontal distal and stable part of the slide and returned an age of 2.5±0.3 ka (DOL-01).
- *Upper valley.* The main ice tongue built a voluminous moraine complex with three frontal ridges ~0.7 km from the current glacier front (Fig. 4A). One lichenized moraine boulder of the outermost well-preserved and stable ridge was sampled at ~400 m a.s.l., yielding an age of 7.1±0.3 (DOL-08). One non-lichenized moraine boulder from the next well-preserved while rounded and wide moraine ridge at ~420 m a.s.l. (Fig. 3) was sampled and returned an exposure age of 0.8±0.1 ka (DOL-07). The closest samples to the ice margin were obtained from one gneiss angular boulder of the horizontal culminating surface of the recent moraine ridge with a ~150-ms length, dropping vertically ~40–50 m to the valley bottom and located ~200 m from the present-day glacier front at ~500 m a.s.l., with an exposure age of 1.9±0.2 ka (DOL-04) (Fig. 4C). A well-preserved medial moraine (2–4-m high) extended for ~160 m between the two most recent moraine complexes which were not sampled owing to a suspicion that they were ice-cored.

Discussion

Our chronological dataset contributes to reconstructing general spatial and temporal patterns with regards to glacial oscillations and climate variability in the region since the onset of the deglaciation. However, some interpretations must be taken with caution as palaeoclimatic studies reconstructing the timing of glacial oscillations in Greenland have reported problems associated with nuclide inheritance and postglacial dynamics affecting the interpretation of the sample results (Kelly *et al.* 2008; Goehring *et al.* 2010; Corbett *et al.* 2013; Farnsworth *et al.* 2018; Skov *et al.* 2020; Biette *et al.* 2020; Larsen *et al.* 2021; Young *et al.* 2021b; Garcia-Oteyza *et al.* 2022).

Considerations on the geochronological dataset

The CRE dates from the Olsen and Dolomit valleys show several chronological inconsistencies with the geomorphological sequences that need to be examined independently in detail in order to assess the validity of the results and their geochronological meaning for the correct interpretation of glacial and postglacial landscape evolution.

For the Olsen Valley, all the inconsistencies detected along the area may reflect different sources of error that will be debated further in the following sections of the discussion: (i) the distortion of moraine ages by GLOFs (dragging of blocks from slopes, removal of blocks, etc.), although the significance of the erosive capacity of GLOFs remains to be defined; (ii) possible ice core moraines that produce a different evolution of the boulders; and (iii) the polished surface samples tending to return older ages than expected owing to inheritance problems.

Among the inconsistencies and some inverted ages detected along the Olsen valley, it is necessary to highlight one polished surface sample from the upper part of the valley that yielded an age of 15.0±0.5 ka (OLS-09), which is stratigraphically inconsistent within the surrounding dated bedrock samples that reported ages ranging from 13.8 to 9.4 ka (OLS-01, OLS-07, OLS-08, OLS-10 and OLS-11). This time range is interpreted

to be associated with ice thinning and the gradual exposure of the landscape to cosmic-ray flux. However, the polished surface sample OLS-09 is significantly out of range and is therefore interpreted to have nuclide inheritance, considered a geomorphological outlier and excluded from the age dataset and further discussion.

The A.P. Olsen Ice Cap has been defined as a cold-based ice cap (Behm *et al*. 2020), which has major implications for past surface erosion. This type of glacier can preserve the signal of past glacial periods and leave behind undisturbed relict landscapes (Fabel *et al*. 2002; Stroeven *et al*. 2002; Sugden *et al*. 2005; Briner *et al*. 2006; Davis *et al*. 2006; Corbett *et al*. 2013), which are a potential source of nuclide inheritance and uncertainties associated with CRE dating as ^{10}Be atoms accumulated from past deglacial periods are often incompletely eliminated as rock surfaces are not eroded deeply enough (Atkins *et al*. 2002). Our dataset for both valleys must be interpreted considering the different erosive capacities of each glacial advance – either because it is a cold-based glacier (insufficient reworking) or because of the brevity of Holocene advances – together with the potential effect of postglacial paraglacial processes in the area. Indeed, this has been identified in the neighbouring Zackenberg Valley where samples provided younger ages than the real deglaciation age owing to postglacial boulder remobilization by rock falls, debris flows, solifluction, etc. (Garcia-Oteyza *et al*. 2022).

For the Dolomit Valley, although some inconsistencies were found, no samples were classified as geomorphologic outliers and therefore all dates were used in the discussion. A comparison of datasets from the two valleys reveals (i) more clustered ages in the Olsen Valley and more scattered ages in the Dolomit Valley (Fig. 5); and (ii) more chemical outliers (five samples) within the Dolomit Valley age dataset than the Olsen Valley (two samples).

One of the main factors explaining these differences might be the lithology of the study areas, which plays a key role in the intensity of (postglacial) periglacial processes affecting the valley slopes. The more weatherable the underlying lithologies (e.g. sedimentary rocks), the more intensely paraglacial processes affect the slopes and their stability. Periglacial processes following glacial retreat have a significant impact on slope mass wasting, which is even more enhanced in permafrost terrain where its effects on different lithologies are highly variable because of pore structure dependence (Gruber & Haeberli 2007) and rock mechanical properties that may control slope destabilization (Krautblatter *et al*. 2013). Soft rocks or porous bedrock (such as sedimentary rocks) are generally more susceptible to frost shattering owing to high porosity and low strength than massive/hard jointed rocks (e.g. metamorphic bedrock) (Murton 2008). All the samples from the Dolomit Valley were obtained in sedimentary bedrock settings that enhanced more intense paraglacial dynamics (e.g. solifluction, alluvial fans, landslides) that destabilized the slopes and favoured the reworking of the samples, thus altering the real deglaciation ages. In contrast, all samples from the Olsen Valley were taken from metamorphic substrates and reflected the lower intensity of mobilization processes on the slopes and, therefore, the greater stability of the landforms and dated boulders. The effect of underlying lithology for CRE dating was also seen in the neighbouring Zackenberg Valley, which showed differences between samples taken on sedimentary (Fig. 6B) and metamorphic (Fig. 6A) slope substrates (Garcia-Oteyza *et al*. 2022). In Zackenberg Valley, the slopes with sedimentary lithology returned more outliers (both chemical and geomorphological) and more scattered ages, while samples on metamorphic substrates returned fewer outliers and more clustered ages (Fig. 6A; Garcia-Oteyza *et al*. 2022). This may indicate that the differences between the age datasets of our two valleys are due, at least in part, to the substrates on which the landforms lay.

Glacial history reconstruction

The geomorphological and geochronological evidence enables the reconstruction of a general chronological history of the deglaciation of these two valleys which can later be compared with the palaeoenvironmental evolution detected across Greenland during T-1 and the Early Holocene.

Olsen Valley. – The final age dataset for the Olsen Valley ranges from 14.3 to 1.1 ka (Fig. 5B). Most of the ages are from polished surfaces spread along the lower, middle and upper parts of the valley and these range from ~14.3 to 9.8 ka, reporting the oldest deglaciation ages from samples located in the lowest parts of the valley. Palaeoclimatically this range is suggesting a rapid ice retreat during the Early Holocene, with a variable ice-cover thickness and disconnection of the glacier valleys from the main ice tongues. The close age differences on the Olsen upper valley polished surface samples (OLS-07 to OLS-11) reinforce the idea of a rapid deglaciation. This general retreat trend was possibly not homogeneous, and it may have included interspersed glacial advances as samples from moraine boulders in the lower and middle valley suggest (12.2±0.4 ka (OLS-04); 9.7±1.2 ka (OLS-05 and OLS-06); 9.4±0.7 ka (OLS-12 and OLS-13)). The remaining two moraine boulder samples are the closest to the current ice front, and state a Late Holocene glacier advance at ~1.5 ka.

Dolomit Valley. – The final age dataset for the Dolomit Valley ranges from 11.4 to 0.7 ka (Fig. 5C). The ages from the lower valley frontal moraine (10.0±1.4 ka (DOL-10, DOL-11 and DOL-12)) confirm that the glacier was already disconnected from Young Sound in the Early Holocene. There is a notable lack of data for the

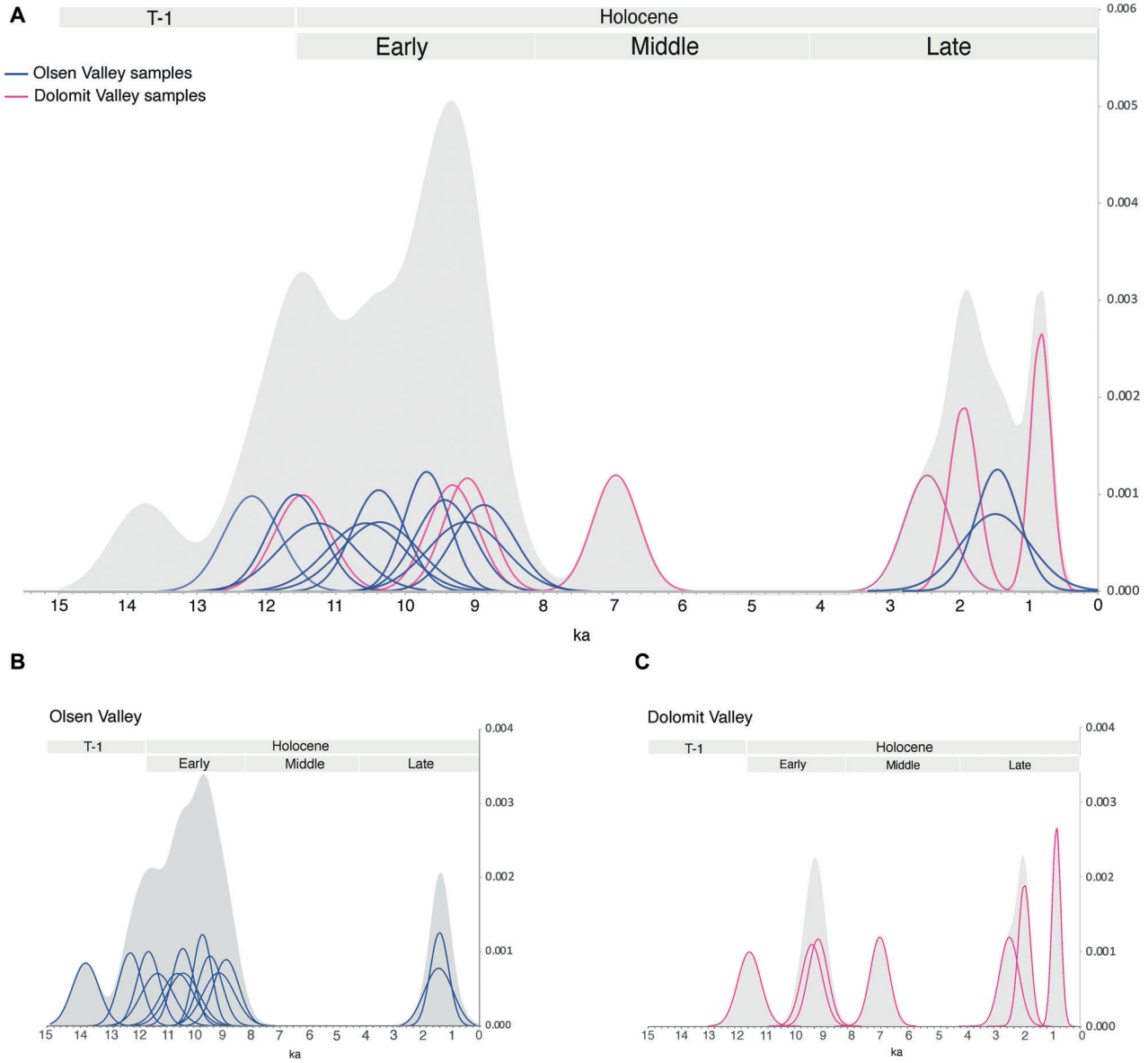

Fig. 5. A. Probability distribution functions of ^{10}Be ages (with internal uncertainties) for all the samples of our final dataset of accepted ages. B. Olsen Valley ^{10}Be age probability distribution function. C. Dolomit Valley ^{10}Be age probability distribution functions.

Middle Holocene in both this valley and the Olsen Valley. Falling under the Middle Holocene period we only found at the upper part of the Dolomit valley a moraine boulder age of 7.0 ka (DOL-08), which fits within the stratigraphy and, despite being just one sample, might mark the retreat of the glacier during the Middle Holocene. The landslide sample at ~2.5 ka suggests that part of the middle valley was already deglaciated at that time and this could mark the age of one of the multiple landslide events that probably occurred throughout the deglaciation. Rapid deglaciation, reaching the upper valley, is indicated by the presence of a well-preserved medial moraine, although the moraine samples in the upper part of the valley also imply that this deglaciation was interrupted by minor advances. The sample closer to the ice front moraine yielded an age of 1.9±0.2 ka (DOL-04), older than the sample from the lower moraine of the system that returned an age of 0.8±0.1 ka (DOL-07). These CRE ages could indicate either that the more distal boulder was moved from its original position, thus resulting in a younger age than might be expected, or that the sample nearest to the ice front boulder may have been affected by inheritance probably associated with insufficient (sub)glacial reworking. Other factors could also have produced this age inversion, including the occurrence of postglacial stabilization of moraine boulders associated with ice-cored moraines or slope readjustment to the new ice-free conditions. As the two

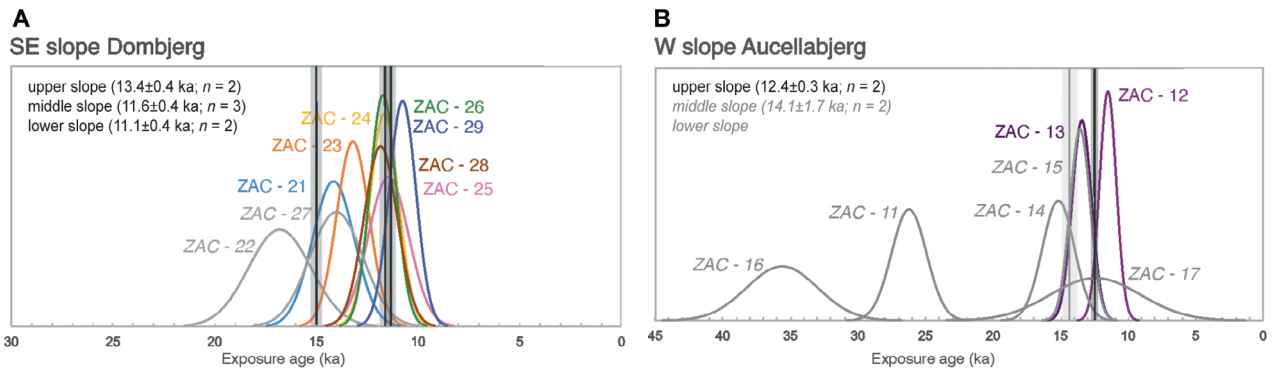

Fig. 6. A. Probability distribution functions of ^{10}Be ages from SE Domjerg slope (Zackenberg Valley) that have metamorphic bedrock. B. Probability distribution functions of ^{10}Be ages from west Aucellabjerg slope (Zackenberg Valley) that have sedimentary bedrock (modified from Garcia-Oteyza *et al.* (2022), see this original publication for the exact location of the samples).

samples were taken close to the glacial front (<1 km), it is likely that both are associated with Neoglacial advances that occurred prior to the LIA.

Glacial oscillations and climate evolution in NE Greenland

The abundance and variety of glacial landforms existing in both valleys down to sea level demonstrate that the area was heavily glaciated during the last glacial cycle. Both valleys were probably filled by ice to the mountain plateaus (up to ~900 m a.s.l.), similar to what occurred in other valleys of the Young Sound–Tyrolerfjord area (Garcia-Oteyza *et al.* 2022, 2023b). The expansion of the GrIS and the surrounding ice caps during the last glacial cycle is well documented in several areas in NE Greenland despite limited chronological control of the sequence of glacial advances and retreats. Prior to the Last Glacial Maximum, between 115 and 75 ka, glacier fronts in this region extended to reach the inner continental shelf (Funder *et al.* 2011; Lecavalier *et al.* 2014). The Olsen and Dolomit valleys must therefore have been occupied by an extensive glacial system interconnected with their tributary valleys feeding the major Young Sound glacier. Direct evidence shows rapid deglaciation following the Last Glacial Maximum in NE Greenland (Ó Cofaigh *et al.* 2004; Hall *et al.* 2008, 2010; Kelly *et al.* 2008; Larsen *et al.* 2010; Möller *et al.* 2010; Funder *et al.* 2011; Vasskog *et al.* 2015).

A number of palaeoclimate records reveal abrupt temperature changes during T-1 (5–15 °C), with a strongly seasonal regime that must have driven changes in GrIS volume (Buizert *et al.* 2014; Vasskog *et al.* 2015). Most of the currently ice-free areas in the southern sector of NE Greenland deglaciated during this period and, broadly across Greenland, the GrIS had already retreated behind the present-day boundaries by 10–9 ka (Carlson *et al.* 2014; Larsen *et al.* 2015; Reusche *et al.* 2018; Lesnek *et al.* 2020; Skov *et al.* 2020; Young *et al.* 2021b). During T-1 through the Early Holocene transition, glacial advances and retreats favoured the formation of multiple moraine ridges at different elevations on slopes and valley bottoms, indicative of rapid climate variability. The long-term retreat and glacial shrinking during T-1 in Greenland was not a continuous process; it included several cold events that favoured readvances or glacial stabilization phases, with periods of moraine formation during the Lateglacial (Carlson *et al.* 2014; Larsen *et al.* 2015; Reusche *et al.* 2018; Skov *et al.* 2020).

Most of our age results from moraine boulders are within the range of 11.5–9.1 ka (Fig. 7). Although more data would be needed to be certain, comparing with the climate periods and events visible on the NGRIP ice core δ^{18}O record (Rasmussen *et al.* 2006) (Fig. 7), two cold events could have influenced the interruption of the long-term deglaciation trend: the Preboreal oscillation (11.5–11.4 ka) and the 9.2 ka event (9.5–9.2 ka interval) (Fig. 7). These abrupt cooling events are well defined in Greenland ice-core isotope records and appear prominently and synchronously in most of them (Kobashi *et al.* 2007; Rasmussen *et al.* 2007; Thomas *et al.* 2007). Both events probably involved the alteration of the Atlantic Meridional Overturning Circulation (AMOC) driven by freshwater input into the North Atlantic Ocean via rapidly melting ice sheets (Renssen *et al.* 2009; Thornalley *et al.* 2018; Jomelli *et al.* 2022). The best known of these events is that at 9.2 ka, for which evidence of a notable climatic anomaly around the Northern Hemisphere is sparse but detectable in multiple palaeorecords (Fleitmann *et al.* 2008), including ^{10}Be moraine chronologies on Baffin Bay region and western Greenland (Crump *et al.* 2020; Young *et al.* 2021a). ^{10}Be CRE studies show that, while brief, this event was of sufficient duration to elicit a significant response by (at least) the western GrIS (Young *et al.* 2013a, 2020). Based on gas-phase temperatures from Greenland ice (Fleitmann *et al.* 2008), the 9.2 ka event is characterized by 2–3 °C mean-annual cooling over ~100 years. The Preboreal oscillation event is less well defined, but this stillstand

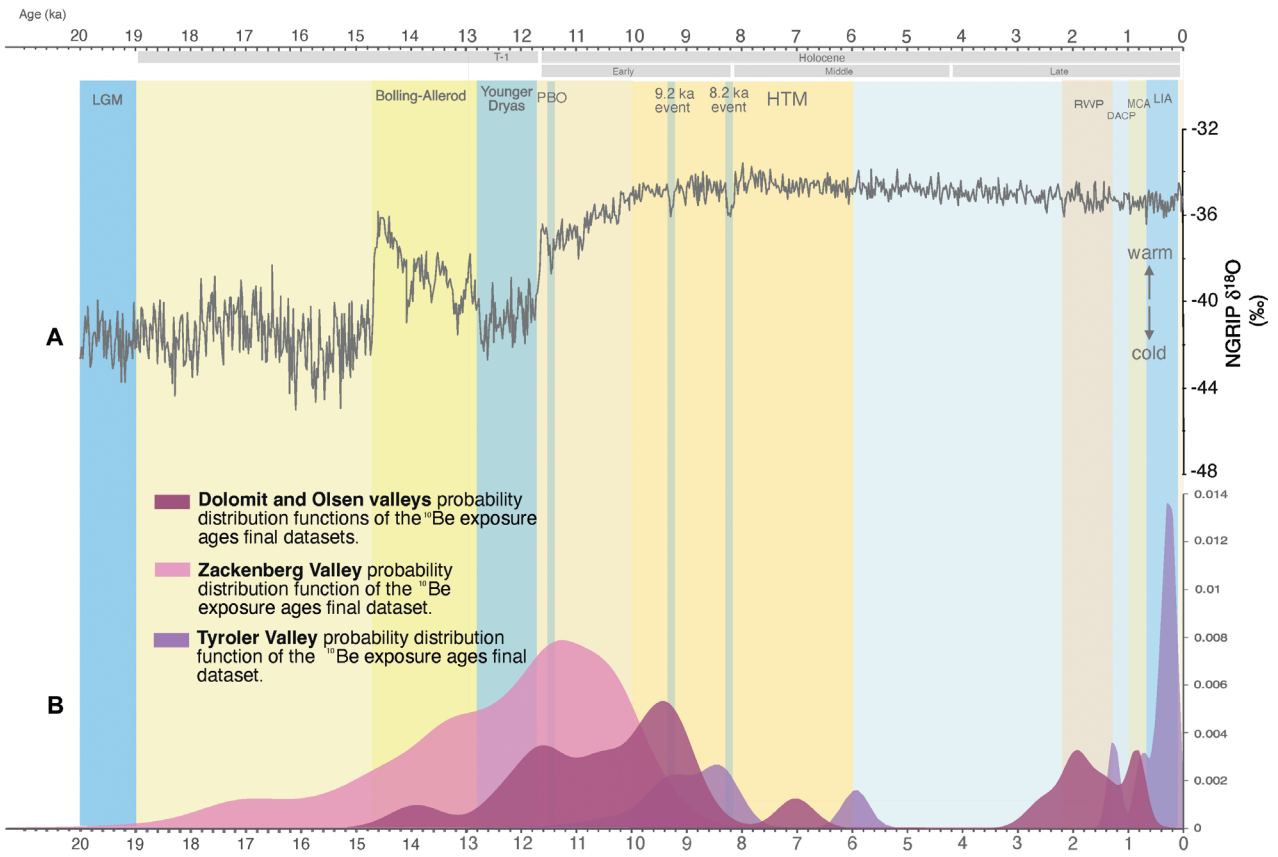

Fig. 7. A. The $\delta^{18}O$ record of the NGRIP ice core smoothed with a 15-interval moving average (GICC05modelext, five-point running mean; Rasmussen *et al.* 2006). B. Sum probability distribution functions of all ^{10}Be ages (Olsen and Dolomit valleys). Sum probability distribution functions of Zackenberg Valley (Garcia-Oteyza *et al.* 2023a, 2023b) and Tyroler Valley (Garcia-Oteyza *et al.* 2023a, 2023b) ^{10}Be ages.

may reflect an interruption of the overall warming near the YD termination in response to a brief episode of freshwater-forced cooling that weakened the AMOC. Similar studies based on ^{10}Be CRE dating detected these events at the GrIS margins in Baffin Bay (Young *et al.* 2020, 2021a), dating stillstands at ~11.6 ka and ~9.1 ka, and in NE Greenland with moraines dated at ~11.4 ka (Levy *et al.* 2016).

Temperatures continued to rise through the Early Holocene (as well marked on the NGRIP record (Fig. 7)) and accelerated the deglaciation pattern observed across Greenland and most Northern Hemisphere glaciers at that time (Clark *et al.* 2012; Buizert *et al.* 2014; Young *et al.* 2021a). The glacial shrinking recorded in our study occurred parallel to increased glacio-isostatic uplift, delta progradation (~13–11 to 6.3 ka) and permafrost aggradation (Christiansen *et al.* 2002; Gilbert *et al.* 2017) in the nearby Zackenberg Valley. Our age assemblages at the end of the Early Holocene denote a rapid glacial retreat in the Dolomit and Olsen valleys, with the deglaciation of the lowest sectors by 11–10 ka. This is consistent with the palaeoclimate reconstructions as well as with previous ^{10}Be CRE chronologies from the neighbouring valleys of the area that show the tributaries disconnecting from the main ice stream at ~11–10 ka in the Zackenberg Valley (Garcia-Oteyza *et al.* 2022) (Fig. 7), at ~10–8.5 ka in the Tyroler Valley (Garcia-Oteyza *et al.* 2023a) (Fig. 7) and after ~10 ka in mountain glaciers in the northern sector of Clavering Island (Biette *et al.* 2020).

As in most areas in NE Greenland, glacial records from the Middle Holocene to the onset of the Late Holocene are absent in the Olsen and Dolomit valleys. In this period glacial fronts were probably situated behind their present positions (Kelly & Lowell 2008; Briner *et al.* 2016). The Holocene Thermal Maximum was a relatively warm phase between 11 and 5 ka commonly associated with the orbitally forced summer insolation maximum but with a spatial and temporal complexity as its timing and magnitude varied between regions and was pronounced at high latitudes (amplified by polar amplification) where its entanglement can be explained by the cooling effect of the Laurentide Ice Sheet, causing delays of 1–2 ka compared WITH the orbitally forced insolation maximum (Renssen *et al.* 2009, 2012). Ice masses across the North Atlantic region, including Greenland, retreated during the Middle Holocene and re-advanced during the Late Holocene mainly owing to changes in the

intensity of the AMOC (Jomelli *et al*. 2022). In Greenland, the GrIS was behind its present-day ice limits at the end of the Holocene Thermal Maximum and during the Middle Holocene, while most peripheral glaciers were smaller than at present or even disappeared completely at that time (Solomina *et al*. 2015). This is also confirmed by other studies in the region, both for mountain glaciers and GrIS margins such as on Clavering Island (Biette *et al*. 2022) and in Tyroler Valley (Garcia-Oteyza *et al*. 2023a), where the lack of geomorphic evidence suggests that glaciers were smaller during most of the Holocene than at present. On the other hand, the fronts of the three terminating outlet glaciers of the NE Greenland Ice Stream, which drains the interior GrIS in the NE region, were behind the present limits from 7.8 to 1.2 ka (Larsen *et al*. 2018), which prolonged the effects of a warm period that this region experienced from 8 to 5 ka (Schmidt *et al*. 2011). In East Greenland glaciers were smaller than they are at present already by ~9.5 ka BP (Medford *et al*. 2021). After ~5 ka there was a general overall decline in temperatures in East Greenland that was interrupted by a series of multi-decadal to century-scale fluctuations (Bradley & Bakke 2019). The NE Greenland Ice Stream expanded during the neoglacial, reaching a maximum at the LIA (Lane *et al*. 2023). In East Greenland glacial advances are evident from ~3.3 ka BP. In fact, the entire GrIS boundary as a whole may have reached its eventual historical maximum extent around 2 ka (Young *et al*. 2021b).

Late Holocene glacial advances have also been CRE dated from the Theodolit Plateau, on west Clavering Island (Biette *et al*. 2020; Jomelli *et al*. 2022), at ~3 ka, 1 ka and the LIA. Around the area, lake sediments also documented glacier advances including from Madsen Lake (~20 km west of Zackenberg), which suggested that three glacier advances occurred over the last 2000 years (Adamson *et al*. 2019), the first two at 1.3 and 0.8 ka, and the third at 0.7 ka. At Aucella Lake in the Zackenberg Valley area, lake sediments documented cold climate conditions at ~3.8–3.4 ka and at ~2.4–2.0 ka with a minimum at ~1.2–0.8 ka and a colder more humid climate at LIA with the maximum glacial extent in the area before ~0.5 ka (Garcia-Oteyza *et al*. 2023b). In Kulusuk (~1000 km south of Zackenberg), sediment cores document glacier advances during Late Holocene, with the most extensive advances occurring at the end of the LIA (Balascio *et al*. 2015).

The most recent CRE sample in Dolomit Valley (0.8±0.1 ka) was from a moraine boulder located ~1 km from the ice front. Although no other results are available to validate this age, it is very similar to that reported ~1000 km south along the NE Greenland coast (Biette *et al*. 2022). These authors reported an early LIA advance at ~0.66–0.70 ka that formed a moraine located at ~500 m from the current ice front. Other studies at Scoresby Sund determined that the ice caps reached the maximum extent during the LIA at ~0.7–0.3 ka (Kelly *et al*. 2008; Levy *et al*. 2014).

Constraints of cosmogenic nuclide dating in Greenland

The problems detected (e.g. age inversion, nuclide inheritance) in the Olsen and Dolomit valley samples have also been detected in the application of CRE methods in Greenland and other Arctic sectors, where cold-based glaciers dominate, the level of continuous or discontinuous permafrost is close to sea level, or where samples are taken at the bottom of valleys under steep slope walls.

Nuclide inheritance may be present but is generally much more limited in the valley bottoms at low altitude (Roberts *et al*. 2013; Skov *et al*. 2020), and comparative studies have shown that nuclide inheritance may or may not be present in neoglacial moraines at the bottom of the valleys (Larsen *et al*. 2021). The level of inheritance largely depends on the entirety of Holocene advances, as in many cases the erosion caused by these advances is unable to completely erase nuclide inventory inherited from previous glacial erosional activity (Larsen *et al*. 2021). This type of lower erosional capacity of these re-advances is more frequent for local mountain glaciers in Greenland, where boulders with ages older than those of the same moraine frequently occur because these re-advance moraines can mix strongly inherited boulders with intensely eroded boulders with no inheritance (Larsen *et al*. 2020, 2021). Although the number of studies on inheritance on bedrock-polished surfaces in valley floors is very limited (Ewertowski & Tomczyk 2015; Bierman *et al*. 2018; Levy *et al*. 2020), the erosive capacity of Holocene reworking on these rock surfaces appears to be decisive in removing cosmogenic nuclides inherited from previous ice-free periods and may largely depend on the degree of weakness of the rock itself (Levy *et al*. 2020). For these reasons, polished bedrock with significant inheritance can be found at the bottom of the valleys where rock strength has prevented the erosion by new glacial advances, and this bedrock surface can be located near other outcrops that have been eroded and do not present inheritance. As such, bedrock outcrops located very close to each other may give ages that differ by 1–3 ka in an illogical geomorphological order (Levy *et al*. 2020; Garcia-Oteyza *et al*. 2022). Another common problem in Greenland and throughout the Arctic is related to the stabilization phases of the Holocene ice-core moraines that are common in these regions. After formation, owing to the uneven insulation capacity of the till, the ice melts under the moraines in an irregular way, which causes an irregular stabilization period of the boulders, and therefore their exposure to cosmogenic radiation is highly variable. As a result of this slow moraine degradation, different CRE ages may be found in the same moraine (Briner *et al*. 2005; Zech *et al*. 2005). In these cases, the oldest ages unaffected by

inheritance are likely to reflect the age of moraine formation (Crump *et al.* 2017).

The other important process that can alter CRE ages is strong post-glacial erosion owing to the importance of steep slope processes, permafrost degradation (Christiansen *et al.* 2008; Rasmussen *et al.* 2018) and intense nival action (Christiansen 1998). These processes can both reset the clock that records ^{10}Be accumulation since glacial sedimentation of boulders and introduce boulders onto the valley floor from higher altitude sectors, where cosmogenic inheritance is more pronounced (Levy *et al.* 2020; Garcia-Oteyza *et al.* 2022). Another important post-glacial process is the GLOFs. They may be common in many Greenland valleys owing to the abundance of proglacial lakes and retreating glacial fronts (Dømgaard *et al.* 2023) and their frequency in the Olsen Valley is well known thanks to the location of the Zackenberg Research Station. In the Olsen Valley, significant GLOFs have been detected with high erosive velocity and power, which have caused significant alterations of the glacial geomorphology of the valley floor (Behm *et al.* 2020; Dømgaard *et al.* 2023). As shown by recent events, GLOFs not only erode and alter the valley floor and sides, but also favour subsequent gravitational processes, destabilizing the slopes (Dømgaard *et al.* 2023).

Conclusions

Despite the limited number of valid CRE ages in Olsen and Dolomit valleys, the general pattern observed in the region of NE Greenland can be confirmed (Fig. S1): (i) rapid deglaciation and disconnection of glaciers from the main glacial systems during the Early Holocene; (ii) no evidence of glacial activity during the Middle Holocene, probably owing to the existence of smaller ice masses than at present; and (iii) glacier expansion during the Late Holocene, with a LIA advance representing the last major period of glacial regrowth. Future studies must complement the chronological framework of these glacial oscillations and the climatic background of these environmental changes.

In the Olsen Valley, which drains the A.P. Olsen Ice Cap, samples collected from moraines tend to be younger than those from polished rock outcrops. This discrepancy can be explained by the fact that the moraines probably underwent a phase as ice-cored moraines, a process that may last several millennia before the boulders fully stabilize. Additionally, the valley frequently experiences GLOFs, which cause significant post-glacial erosion of the moraines. These processes contribute to the younger-than-expected CRE ages of the moraines, owing to the exhumation or overturning of boulders. In contrast, the outlet glacier descending the valley has a cold base, limiting its erosive capacity. As a result, ages obtained from polished rock outcrops tend to be older than expected, with some being particularly anomalous outliers. Nevertheless, the Olsen Valley was probably deglaciated from approximately ~14.3 ka onwards, with significant activity during the Early Holocene, around ~9.8 ka. The glacier advanced around ~1.5 ka before retreating once again.

The glacier down the Dolimit Valley was already disconnected from the main fjord by ~10.0 ka. The glacier had left the middle valley as early as ~2.5 ka, the age of a landslide that occupies this sector of the valley. The glacier advanced again between ~1.9 and 0.8 ka.

Acknowledgements. – This study was funded by the NEOGREEN (PID2020-113798GB-C31) and PALEOGREEN (CTM2017-87976-P) projects of the Spanish Ministerio de Economía y Competitividad. Field research was also supported by the research group ANTALP (Antarctic, Arctic, Alpine Environments; 2017-SGR-1102) funded by the Agència de Gestio d'Ajuts Universitaris i de Recerca of the Government of Catalonia. Julia Garcia-Oteyza was supported by an FPI fellowship from the Spanish Ministry of Science. The ^{10}Be measurements were performed at the ASTER AMS national facility (CEREGE, Aix-en-Provence), which is supported by the INSU/CNRS and the ANR through the 'Projets thématiques d'excellence' programme for the 'Equipements d'excellence' ASTER-CEREGE action and IRD. We are also grateful to Jesús Ruiz and Zackenberg Research Station for field support.

Author contributions. – JG-O: writing of the first draft of the manuscript, fieldwork leading, geomorphological analysis and mapping, laboratory tasks (sample processing, exposure age calculations) and data processing. MO: fieldwork, funding acquisition, geomorphological analysis, contribution to the writing, and revision of the final manuscript. DP: geomorphological analysis, contribution to the writing, and revision of the final manuscript. JMF-F: laboratory tasks (sample processing, exposure age calculations), data processing, contribution to the writing and revision of the final manuscript. IS: sample processing supervision, interpretation of the results and revision of the final manuscript. MF: data discussion and revision of the final manuscript. SG: data discussion and revision of the final manuscript. DA: data discussion and revision of the final manuscript. VJ: revision of the final manuscript.

Data availability statement. – On behalf of the authors, I declare the data will be available to anyone interested any time on request.

References

Adamson, K., Lane, T., Carney, M., Bishop, T. & Delaney, C. 2019: High-resolution proglacial lake records of pre-Little Ice Age glacier advance, northeast Greenland. *Boreas 48*, 535–550.

Atkins, C., Barrett, P. & Hicock, S. 2002: Cold glaciers erode and deposit: evidence from Allan Hills, Antarctica. *Geology 30*, 659–662.

Balascio, N. L., D'Andrea, W. J. & Bradley, R. S. 2015: Glacier response to North Atlantic climate variability during the Holocene. *Climate of the Past 11*, 1587–1598, https://doi.org/10.5194/cp-11-1587-2015.

Balco, G. 2019: Glacier change and paleoclimate applications of cosmogenic-nuclide exposure dating. *Annual Review of Earth and Planetary Sciences 48*, 1–28.

Balco, G., Stone, J. O., Lifton, N. A. & Dunai, T. J. 2008: A complete and easily accessible means of calculating surface exposure ages or erosion rates from ^{10}Be and ^{26}Al measurements. *Quaternary Geochronology 3*, 174–195.

Behm, M., Walter, J. I., Binder, D., Cheng, F., Citterio, M., Kulessa, B., Langley, K., Limpach, P., Mertl, S., Schöner, W., Tamstorf, M. & Weyss, G. 2020: Seismic characterization of a rapidly-rising jökulhlaup cycle at the A.P. Olsen Ice Cap, NE-Greenland. *Journal of Glaciology 66*, 329–347.

Bierman, P. R., Corbett, L. B., Graly, J. A., Neumann, T. A., Lini, A., Crosby, B. T. & Rood, D. H. 2014: Preservation of a preglacial landscape under the center of the Greenland Ice Sheet. *Science 344*, 402–405.

Bierman, P. R., Rood, D. H., Shakun, J. D., Portenga, E. W. & Corbett, L. B. 2018: Directly dating postglacial Greenlandic land-surface emergence at high resolution using in situ ^{10}Be. *Quaternary Research 90*, 110–126.

Biette, M., Jomelli, V., Chenet, M., Braucher, R., Rinterknecht, V. & Lane, T. 2020: Mountain glacier fluctuations during the Lateglacial and Holocene on Clavering Island (northeastern Greenland) from ^{10}Be moraine dating. *Boreas 49*, 873–885.

Biette, M., Jomelli, V., Chenet, M., Braucher, R., Menviel, L., Swingedouw, D., Rinterknecht, V. & ASTER Team 2022: Evidence of the largest Late Holocene mountain glacier extent in southern and southeastern Greenland during the middle Neoglacial from 10Be moraine dating. *Boreas 51*, 61–77, https://doi.org/10.1111/bor.12555.

Bjørk, A. A., Aagaard, S., Lütt, A., Khan, S. A., Box, J. E., Kjeldsen, K. K., Larsen, N. K., Korsgaard, N. J., Cappelen, J., Colgan, W. T., Machguth, H., Andresen, C. S., Peings, Y. & Kjær, K. H. 2018: Changes in Greenland's peripheral glaciers linked to the North Atlantic Oscillation. *Nature Climate Change 8*, 48–52.

Bradley, R. S. & Bakke, J. 2019: Is there evidence for a 4.2 ka BP event in the northern North Atlantic region? *Climate of the Past 15*, 1665–1676.

Briner, J. P., Kaufman, D. S., Manley, W. F., Finkel, R. C. & Caffee, M. W. 2005: Cosmogenic exposure dating of late Pleistocene moraine stabilization in Alaska. *GSA Bulletin 117*, 1108–1120.

Briner, J. P., Mckay, N. P., Axford, Y., Bennike, O., Bradley, R. S., Vernal, A. D., Fisher, D., Francus, P., Fréchette, B., Gajewski, K., Jennings, A., Kaufman, D. S., Miller, G., Rouston, C. & Wagner, B. 2016: Holocene climate change in Arctic Canada and Greenland. *Quaternary Science Reviews 147*, 340e364, https://doi.org/10.1016/j.quascirev.2016.02.010.

Briner, J. P., Miller, G. H., Davis, P. T. & Finkel, R. C. 2006: Cosmogenic radionuclides from fiord landscapes support differential erosion by overriding ice sheets. *GSA Bulletin 118*, 406–420.

Buizert, C., Gkinis, V., Severinghaus, J. P., He, F., Lecavalier, B. S., Kindler, P., Leuenberger, M., Carlson, A. E., Vinther, B., Masson-Delmotte, V., White, J. W. C., Liu, Z., Otto-Bliesner, B. & Brook, E. J. 2014: Greenland temperature response to climate forcing during the last deglaciation. *Science 80*, 1177–1180.

Buus-Hinkler, J., Hansen, B. U., Tamstorf, M. P. & Pedersen, S. B. 2006: Snow-vegetation relations in a High Arctic ecosystem: inter-annual variability inferred from new monitoring and modeling concepts. *Remote Sensing of Environment 105*, 237–247.

Carlson, A. E., Winsor, K., Ullman, D. J., Brook, E. J., Rood, D. H., Axford, Y., LeGrande, A. N., Anslow, F. S. & Sinclair, G. 2014: Earliest Holocene south Greenland ice sheet retreat within its late Holocene extent. *Geophysical Research Letters 41*, 5514–5521.

CAVM Team 2003: Circumpolar Arctic Vegetation Map. (1:7,500,000 scale), Conservation of Arctic Flora and Fauna (CAFF) Map No. 1. US Fish Wildl. Serv. AK. https://www.Geobot.uaf.edu/cavm/ [Verified 1 August 15 July 2015] 2.

Christiansen, H. H. 1998: Nivation forms and processes in unconsolidated sediments, NE Greenland. *Earth Surface Processes and Landforms 23*, 751–760.

Christiansen, H. H., Bennike, O., Böcher, J., Elberling, B., Humlum, O. & Jakobsen, B. H. 2002: Holocene environmental reconstruction from deltaic deposits in Northeast Greenland. *Journal of Quaternary Science 17*, 145–160.

Christiansen, H. H., Sigsgaard, C., Humlum, O., Rasch, M. & Hansen, B. U. 2008: Permafrost and Periglacial Geomorphology at Zackenberg. *Advances in Ecological Research 40*, 151–174.

Christoffersen, K. S., Amsinck, S. L., Landkildehus, F., Lauridsen, T. L. & Jeppesen, E. 2008a: Lake flora and fauna in relation to ice-melt, water temperature and chemistry at Zackenberg. *Advances in Ecological Research 40*, 371–389, https://doi.org/10.1016/S00652504(07)00016-5.

Christoffersen, P., Jacobs, K., Ornthanalai, C. & Wang, Y. 2008b: Option valuation with long-run and short-run volatility components. *Journal of Financial Economics 90* (3), 272–297, https://doi.org/10.1016/j.jfineco.2007.12.003.

Clark, P. U. and 30 others 2012: Global climate evolution during the last deglaciation. *Proceedings of the National Academy of Sciences of the United States of America 19*, E1134–E1142, https://doi.org/10.1073/pnas.1116619109.

Corbett, L. B., Bierman, P. R., Graly, J. A., Neumann, T. A. & Rood, D. H. 2013: Constraining landscape history and glacial Erosivity using paired cosmogenic nuclides in Upernavik, Northwest Greenland. *Geological Society of America Bulletin 125*, 9–11.

Crump, S. E., Anderson, L. S., Miller, G. H. & Anderson, R. S. 2017: Interpreting exposure ages from ice-cored moraines: a Neoglacial case study on Baffin Island, Arctic Canada. *Journal of Quaternary Science 32*, 1049–1062.

Crump, S. E., Young, N. E., Miller, G. H., Pendleton, S. L., Tulenko, J. P., Anderson, R. S. & Briner, J. P. 2020: Glacier expansion on Baffin Island during early Holocene cold reversals. *Quaternary Science Reviews 241*, 106419, https://doi.org/10.1016/j.quascirev.2020.106419.

Davis, P. T., Briner, J. P., Coulthard, R. D., Finkel, R. W. & Miller, G. H. 2006: Preservation of Arctic landscapes overridden by cold-based ice sheets. *Quaternary Research 65*, 156–163.

Dømgaard, M., Kjeldsen, K. K., Huiban, F., Carrivick, J. L., Khan, S. A. & Bjørk, A. A. 2023: Recent changes in drainage route and outburst magnitude of the Russell Glacier ice-dammed lake, West Greenland. *The Cryosphere 17*, 1373–1387.

Elberling, B., Tamstorf, M. P., Sigsgaard, C., Illeris, L., Bay, C., Hansen, B. H., Christensen, T. R., Hansen, E. S., Jakobsen, B. H. & Beyens, L. 2008: Soil and plant community-characteristics and dynamics at Zackenberg. *Advances in Ecological Research 40*, 223–248.

Ewertowski, M. W. & Tomczyk, A. M. 2015: Quantification of the ice-cored moraines' short-term dynamics in the high-Arctic glaciers Ebbabreen and Ragnarbreen, Petuniabukta, Svalbard. *Geomorphology 234*, 211–227.

Fabel, D., Stroeven, A. P., Harbor, J., Kleman, J., Elmore, D. & Fink, D. 2002: Landscape preservation under fennoscandian ice sheets determined from in situ produced ^{10}Be and ^{26}Al. *Earth and Planetary Science Letters 201*, 397–406.

Farnsworth, L. B., Kelly, M. A., Bromley, G. R. M., Axford, Y., Osterberg, E. C., Howley, J. A., Jackson, M. S. & Zimmerman, S. R. 2018: Holocene history of the Greenland Ice-Sheet margin in Northern Nunatarssuaq, Northwest Greenland. *Arktos 4*, 1–27.

Fleitmann, D., Mudelsee, M., Burns, S. J., Bradley, R. S., Kramers, J. & Matter, A. 2008: Evidence for a widespread climatic anomaly at around 9.2 ka before present. *Paleoceanography 23*, PA 1102, https://doi.org/10.1029/2007PA001519.

Funder, S., Kjeldsen, K. K., Kjær, K. H. & Ó Cofaigh, C. 2011: The Greenland Ice Sheet during the past 300,000 years: a review. *Developments in Quaternary Sciences 15*, 699–713.

Garcia-Oteyza, J., Giralt, S., Pla-Rabes, S., Antoniades, D., Oliva, M., Ghanbari, H., Osorio-Serrano, R. & Palacios, D. 2023a: A ∼5000 year multiproxy record of summer climate in NE Greenland. *Science of the Total Environment 906*, 167713, https://doi.org/10.1016/j.scitotenv.2023.167713.

Garcia-Oteyza, J., Oliva, M., Palacios, D., Fernández-Fernández, J. M., Schimmelpfennig, I., Andrés, N., Antoniades, D., Christiansen, H. H., Humlum, O., Léanni, L., Jomelli, V., Ruiz-Fernández, J., Rinterknecht, V., Lane, T. P., Adamson, K., Aumaître, G., Bourlès, D. & Keddadouche, K. 2022: Late Glacial deglaciation of the Zackenberg area, NE Greenland. *Geomorphology 401*, 108125, https://doi.org/10.1016/j.geomorph.2022.108125.

Garcia-Oteyza, J., Oliva, M., Palacios, D., Schimmelpfennig, I., Medialdea, A., Fernández-fernández, J. M., Fernandes, M., Giralt, S., Jomelli, V., Antoniades, D. & Team, A. 2023b: Holocene glacial oscillations in the Tyroler Valley (NE Greenland). *Land Degradation & Development 34*, 2589–2606.

Gilbert, G. L., Cable, S., Thiel, C., Christiansen, H. H. & Elberling, B. 2017: Cryostratigraphy, sedimentology, and the late Quaternary evolution of the Zackenberg River delta, northeast Greenland. *The Cryosphere 11*, 1265–1282.

Goehring, B. M., Kelly, M. A., Schaefer, J. M., Finkel, R. C. & Lowell, T. V. 2010: Dating of raised marine and lacustrine deposits in east Greenland using beryllium-10 depth profiles and implications for

estimates of subglacial erosion. *Journal of Quaternary Science 25*, 865–874.
Gosse, J. & Klein, J. 2014: Terrestrial cosmogenic nuclide dating. *In* Rink, W. & Thompson, J. (eds.): *Encyclopedia of Scientific Dating Methods*, 1–23. EEUU: Springer, https://doi.org/10.1007/978-94-007-6326-5_148-1.
Grønnow, B., Jensen, J. F., Sørensen, M., Gullov, H. C., Gotfredsen, A. B. & Melgaard, M. 2009: Geographical report of the GeoArk expeditions to north-East Greenland 2007 and 2008. *SILA – National Museum of Denmark 29*, 1–90.
Gruber, S. & Haeberli, W. 2007: Permafrost in steep bedrock slopes and its temperatures-related destabilization following climate change. *Journal of Geophysical Research 112*, 1–10.
Håkansson, L., Alexanderson, H., Hjort, C., Möller, P., Briner, J. P. & Possnert, A. A. 2009: Late Pleistocene glacial history of Jameson land, central East Greenland, derived from cosmogenic ^{10}Be and ^{26}Al exposure dating. *Boreas 38*, 244–260.
Håkansson, L., Briner, J. P., Aldahan, A. & Possnert, G. 2011: ^{10}Be data from meltwater channels suggest that Jameson land, east Greenland, was ice-covered during the last glacial maximum. *Quaternary Research 76*, 452–459.
Håkansson, L., Briner, J., Alexanderson, H., Aldahan, A. & Possnert, G. 2007: ^{10}Be ages from central east Greenland constrain the extent of the Greenland ice sheet during the Last Glacial Maximum. *Quaternary Science Reviews 26*, 2316–2321.
Hall, B. L., Baroni, C. & Denton, G. H. 2010: Relative sea-level changes, Schuchert Dal, East Greenland, with implications for ice extent in late-glacial and Holocene times. *Quaternary Science Reviews 29* (25–26), 3370–3378, https://doi.org/10.1016/j.quascirev.2010.03.013.
Hall, B., Baroni, C., Denton, G., Kelly, M. A. & Lowell, T. 2008: Relative sea-level change, Kjove Land, Scoresby Sund, East Greenland: implications for seasonality in Younger Dryas time. *Quaternary Science Reviews 27*, 2283–2291.
Hansen, B. U., Sigsgaard, C., Rasmussen, L., Cappelen, J., Hinkler, J., Mernild, S. H., Petersen, D., Tamstorf, M. P., Rasch, M. & Hasholt, B. 2008: Present-day climate at Zackenberg. *Advances in Ecological Research 40*, 111–149.
Hinkler, J., Hansen, B. U., Tamstorf, M. P., Sigsgaard, C. & Petersen, D. 2008: Snow and snow-cover in central Northeast Greenland. *Advances in Ecological Research 40*, 175–195.
Højlund Pedersen, S. 2017: *Scaling-up Climate Change Effects in Greenland*. Ph.D. thesis, Aarhus University, 178 pp.
IMBIE Team 2020: Mass balance of the Greenland Ice Sheet from 1992 to 2018. *Nature 579*, 233–239.
Jomelli, V., Swingedouw, D., Vuille, M., Favier, V., Goehring, B., Shakun, J., Braucher, R., Schimmelpfennig, I., Menviel, L., Rabatel, A., Martin, L. C. P., Blard, P. H., Condom, T., Lupker, M., Christl, M., He, Z., Verfaillie, D., Gorin, A., Aumaître, G., Bourlès, D. L. & Keddadouche, K. 2022: In-phase millennial-scale glacier changes in the tropics and North Atlantic regions during the Holocene. *Nature Communications 13*, 1–11.
Kelly, M. A. & Lowell, T. V. 2008: Fluctuations of local glaciers in Greenland during latest Pleistocene and Holocene time. *Quaternary Science Reviews 28*, 2088–2106.
Kelly, M. A., Lowell, T. V., Hall, B. L., Schaefer, J. M., Finkel, R. C., Goehring, B. M., Alley, R. B. & Denton, G. H. 2008: A ^{10}Be chronology of lateglacial and Holocene mountain glaciation in the Scoresby Sund region, east Greenland: implications for seasonality during lateglacial time. *Quaternary Science Reviews 27*, 2273–2282.
Khan, S. A., Colgan, W., Neumann, T. A., van den Broeke, M. R., Brunt, K. M., Noël, B., Bamber, J. L., Hassan, J. & Bjørk, A. A. 2022: Accelerating ice loss from peripheral glaciers in North Greenland. *Geophysical Research Letters 49*, e2022GL098915, https://doi.org/10.1029/2022GL098915.
King, M. D., Howat, I. M., Candela, S. G., Noh, M. J., Jeong, S., Noël, B. P. Y., van den Broeke, M. R., Wouters, B. & Negrete, A. 2020: Dynamic ice loss from the Greenland Ice Sheet driven by sustained glacier retreat. *Communications Earth & Environment 1*, 1–7.
Kobashi, T., Severinghaus, J. P., Brook, E. J., Barnola, J. M. & Grachev, A. M. 2007: Precise timing and characterization of abrupt climate change 8200 years ago from air trapped in polar ice. *Quaternary Science Reviews 26*, 1212–1222.
Koch, L. & Haller, J. 1971: Geological map of East Greenland 72°-76 °N. *Meddelelser om Grønland 183*, 1–26.
Krautblatter, M., Funk, D. & Günzel, F. K. 2013: Why permafrost rocks become unstable: a rock-ice-mechanical model in time and space. *Earth Surface Processes and Landforms 38*, 876–887.
Kroon, A., Abermann, J., Bendixen, M., Lund, M., Sigsgaard, C., Skov, K. & Hansen, B. U. 2017: Deltas, freshwater discharge, and waves along the Young Sound, NE Greenland. *Ambio 46*, 132–145.
Lal, D. 1991: Cosmic ray labeling of erosion surfaces: in situ nuclide production rates and erosion models. *Earth and Planetary Science Letters 104*, 424–439.
Lane, T. P., Darvill, C., Rea, B. R., Bentley, M. J., Smith, J. A. & Jamieson, S. S. R. 2023: The geomorphological record of an ice stream to ice shelf transition in Northeast Greenland. *Earth Surface Processes and Landforms 7*, 1321–1341.
Larsen, N. K., Kjær, K. H., Funder, S., Möller, P., van der Meer, J. J. M., Schomacker, A., Linge, H. & Darby, D. A. 2010: Late Quaternary glaciation history of northernmost Greenland – evidence of shelf-based ice. *Quaternary Science Reviews 29*, 3399–3414.
Larsen, N. K., Kjær, K. H., Lecavalier, B., Bjørk, A. A., Colding, S., Huybrechts, P., Jakobsen, K. E., Kjeldsen, K. K., Knudsen, K. L., Odgaard, B. V. & Olsen, J. 2015: The response of the southern Greenland ice sheet to the Holocene thermal maximum. *Geology 43*, 291–294.
Larsen, N. K., Levy, L. B., Carlson, A. E., Buizert, C., Olsen, J., Strunk, A., Bjørk, A. A. & Skov, D. S. 2018: Instability of the Northeast Greenland Ice Stream over the last 45,000 years. *Nature Communications 9*, 3–10.
Larsen, N. K., Søndergaard, A. S., Levy, L. B., Laursen, C. H., Bjørk, A. A., Kjeldsen, K. K., Funder, S., Strunk, A., Olsen, J. & Kjær, K. H. 2021: Cosmogenic nuclide inheritance in Little Ice Age moraines – a case study from Greenland. *Quaternary Geochronology 65*, 101200, https://doi.org/10.1016/j.quageo.2021.101200.
Larsen, N. K., Søndergaard, A. S., Levy, L. B., Olsen, J., Strunk, A., Bjørk, A. A. & Skov, D. 2020: Contrasting modes of deglaciation between fjords and inter-fjord areas in eastern North Greenland. *Boreas 49*, 903–917.
Lecavalier, B. S., Milne, G. A., Simpson, M. J. R., Wake, L., Huybrechts, P., Tarasov, L., Kjeldsen, K. K., Funder, S., Long, A. J., Woodroffe, S., Dyke, A. S. & Larsen, N. K. 2014: A model of Greenland ice sheet deglaciation constrained by observations of relative sea level and ice extent. *Quaternary Science Reviews 102*, 54–84.
Leger, T. P. M., Clark, C. D., Huynh, C., Jones, S., Ely, J. C., Sarah, L., Diemont, C. & Hughes, A. L. C. 2023: A Greenland-wide empirical reconstruction of paleo ice-sheet retreat informed by ice extent markers: PaleoGrIS version 1.01-97.
Lenton, T. M., Held, H., Kriegler, E., Hall, J. W., Lucht, W., Rahmstorf, S. & Schellnhuber, H. J. 2008: Tipping elements in the Earth's climate system. *Proceedings of the National Academy of Sciences of the United States of America 105*, 1786–1793.
Lesnek, A. J., Briner, J. P., Young, N. E. & Cuzzone, J. K. 2020: Maximum Southwest Greenland Ice Sheet Recession in the Early Holocene. *Geophysical Research Letters 47*, 1–11.
Levy, L. B., Kelly, M. A., Lowell, T. V., Hall, B. L., Hempel, L. A., Honsaker, W. M., Lusas, A. R., Howley, J. A. & Axford, Y. L. 2014: Holocene fluctuations of Bregne ice cap, Scoresby Sund, east Greenland: a proxy for climate along the Greenland Ice Sheet margin. *Quaternary Science Reviews 92*, 357–368.
Levy, L. B., Kelly, M. A., Lowell, T. V., Hall, B. L., Howley, J. A. & Smith, C. A. 2016: Coeval fluctuations of the Greenland ice sheet and a local glacier, central East Greenland, during late glacial and early Holocene time. *Geophysical Research Letters 43*, 1623–1631.
Levy, L. B., Larsen, N. K., Knudsen, M. F., Egholm, D. L., Bjørk, A. A., Kjeldsen, K. K., Kelly, M. A., Howley, J. A., Olsen, J., Tikhomirov, D., Zimmerman, S. R. H. & Kjær, K. H. 2020: Multi-phased deglaciation of south and southeast Greenland controlled by climate and topographic setting. *Quaternary Science Reviews 242*, 106454, https://doi.org/10.1016/j.quascirev.2020.106454.
López-Blanco, E., Jackowicz-Korczynski, M., Mastepanov, M., Skov, K., Westergaard-Nielsen, A., Williams, M. & Christensen, T. R. 2020: Multi-year data-model evaluation reveals the importance of nutrient availability over climate in arctic ecosystem C dynamics.

Environmental Research Letters 15, 94007, https://doi.org/10.1088/1748-9326/ab865b.
Lowell, T. V., Hall, B. L., Kelly, M. A., Bennike, O., Lusas, A. R., Honsaker, W., Smith, C. A., Levy, L. B., Travis, S. & Denton, G. H. 2013: Late Holocene expansion of Istorvet ice cap, Liverpool Land, east Greenland. *Quaternary Science Reviews 63*, 128–140.
Medford, A. K., Hall, B. L., Lowell, T. V., Kelly, M. A., Levy, L. B., Wilcox, P. S. & Axford, Y. 2021: Holocene glacial history of Renland Ice Cap, East Greenland, reconstructed from lake sediments, 106883. *Quaternary Science Reviews 258*, 106883. https://doi.org/10.1016/j.quascirev.2021.106883.
Meredith, M., Sommerkorn, M., Cassotta, S., Derksen, C., Ekaykin, A. & Hollowed, A. 2019: Polar regions. IPCC special report on the Ocean and cryosphere in a changing climate, 203–320.
Möller, P., Larsen, N. K., Kjær, K. H., Funder, S., Schomacker, A., Linge, H. & Fabel, D. 2010: Early to middle Holocene valley glaciations on northernmost Greenland. *Quaternary Science Reviews 29*, 3379–3398.
Murton, M. 2008: Remote sensing of rermafrost-related problems and hazards. *Permafrost and Periglacial Processes 136*, 107–136.
Ó Cofaigh, C., Dowdeswell, J. A., Evans, J., Kenyon, N. H., Taylor, J., Mienert, J. & Wilken, M. 2004: Timing and significance of glacially influenced mass-wasting in the submarine channels of the Greenland Basin. *Marine Geology 207*, 39–54.
Paxman, G. J. G., Jamieson, S. S. R., Dolan, A. M. & Bentley, M. J. 2024: Subglacial valleys preserved in the highlands of south and east Greenland record restricted ice extent during past warmer climates. *The Cryosphere 18*, 1467–1493.
Porter, C., Morin, P., Howat, I., Noh, M.-J., Bates, B., Peterman, K., Keesey, S., Schlenk, M., Gardiner, J., Tomko, K., Willis, M., Kelleher, C., Cloutier, M., Husby, E., Foga, S., Nakamura, H., Platson, M., Michael Wethington, C. W., Jr., Bauer, G. and 20 others 2018: ArcticDEM.
Rasmussen, S. O., Andersen, K. K., Svensson, A. M., Steffensen, J. P., Vinther, B. M., Clausen, H. B., Siggaard-Andersen, M. L., Johnsen, S. J., Larsen, L. B., Dahl-Jensen, D., Bigler, M., Röthlisberger, R., Fischer, H., Goto-Azuma, K., Hansson, M. E. & Ruth, U. 2006: A new Greenland ice core chronology for the last glacial termination. *Journal of Geophysical Research 111*, 1–16.
Rasmussen, S. O., Vinther, B. M., Clausen, H. B. & Andersen, K. K. 2007: Early Holocene climate oscillations recorded in three Greenland ice cores. *Quaternary Science Reviews 26*, 1907–1914.
Rasmussen, L. H., Zhang, W., Hollesen, J., Cable, S., Christiansen, H. H., Jansson, P. E. & Elberling, B. 2018: Modelling present and future permafrost thermal regimes in Northeast Greenland. *Cold Regions Science and Technology 146*, 199–213.
Renssen, H., Seppä, H., Crosta, X., Goosse, H. & Roche, D. M. 2012: Global characterization of the Holocene Thermal Maximum. *Quaternary Science Reviews 48*, 7–19.
Renssen, H., Seppä, H., Heiri, O., Roche, D. M., Goosse, H. & Fichefet, T. 2009: The spatial and temporal complexity of the holocene thermal maximum. *Nature Geoscience 2*, 411–414.
Reusche, M. M., Marcott, S. A., Ceperley, E. G., Barth, A. M., Brook, E. J., Mix, A. C. & Caffee, M. W. 2018: Early to Late Holocene surface exposure ages from two marine-terminating outlet glaciers in Northwest Greenland. *Geophysical Research Letters 45*, 7028–7039.
Roberts, D. H., Rea, B. R., Lane, T. P., Schnabel, C. & Rodés, A. 2013: New constraints on Greenland ice sheet dynamics during the last glacial cycle: evidence from the Uummannaq ice stream system. *Journal of Geophysical Research: Earth Surface 118*, 519–541.
Schmidt, S., Wagner, B., Heiri, O., Klug, M., Bennike, O. & Melles, M. 2011: Chironomids as indicators of the Holocene climatic and environmental history of two lakes in Northeast Greenland. *Boreas 40*, 116–130, https://doi.org/10.1111/j.1502-3885.2010.00173.x.
Skov, D. S., Andersen, J. L., Olsen, J., Jacobsen, B. H., Knudsen, M. F., Jansen, J. D., Larsen, N. K. & Egholm, D. L. 2020: Constraints from cosmogenic nuclides on the glaciation and erosion history of Dove Bugt, northeast Greenland. *Bulletin of Geological of the American Society 132*, 2282–2294.
Solomina, O. N., Bradley, R. S., Hodgson, D. A., Ivy-Ochs, S., Jomelli, V., Mackintosh, A. N., Nesje, A., Owen, L. A., Wanner, H., Wiles, G. C. & Young, N. E. 2015: Holocene glacier fluctuations. *Quaternary Science Reviews 111*, 9–34.
Stone, J. O. 2000: Air pressure and cosmogenic isotope production. *Journal of Geophysical Research 105*, 753–759.
Stroeven, A. P., Fabel, D., Harbor, J., Hättestrand, C. & Kleman, J. 2002: Quantifying the erosional impact of the fennoscandian ice sheet in the torneträsk–narvik corridor, northern Sweden, based on cosmogenic radionuclide data. *Geografiska Annaler: Series A, Physical Geography 84* (3–4), 275–287, https://doi.org/10.1111/j.0435-3676.2002.00182.x.
Sugden, D. E., Balco, G., Cowdery, S. G., Stone, J. O. & Sass, L. C. 2005: Selective glacial erosion and weathering zones in the coastal mountains of Marie Byrd Land, Antarctica. *Geomorphology 67*, 317–334.
Thomas, E. R., Wolff, E. W., Mulvaney, R., Steffensen, J. P., Johnsen, S. J., Arrowsmith, C., White, J. W. C., Vaughn, B. & Popp, T. 2007: The 8.2 ka event from Greenland ice cores. *Quaternary Science Reviews 26*, 70–81.
Thornalley, D. J. R., Oppo, D. W., Ortega, P., Robson, J. I., Brierley, C. M., Davis, R., Hall, I. R., Moffa-Sanchez, P., Rose, N. L., Spooner, P. T., Yashayaev, I. & Keigwin, L. D. 2018: Anomalously weak Labrador Sea convection and Atlantic overturning during the past 150 years. *Nature 556*, 227–230.
Vasskog, K., Langebroek, P. M., Andrews, J. T., Nilsen, J. E. Ø. & Nesje, A. 2015: The Greenland Ice Sheet during the last glacial cycle: current ice loss and contribution to sea-level rise from a palaeoclimatic perspective. *Earth-Science Reviews 150*, 45–67.
Young, N. E., Briner, J. P., Miller, G. H., Lesnek, A. J., Crump, S. E., Pendleton, S. L., Schwartz, R. & Schaefer, J. M. 2021a: Pulsebeat of early Holocene glaciation in Baffin Bay from high-resolution beryllium-10 moraine chronologies. *Quaternary Science Reviews 270*, 107179, https://doi.org/10.1016/j.quascirev.2021.107179.
Young, N. E., Briner, J. P., Miller, G. H., Lesnek, A. J., Crump, S. E., Thomas, E. K., Pendleton, S. L., Cuzzone, J., Lamp, J., Zimmerman, S., Caffee, M. & Schaefer, J. M. 2020: Deglaciation of the Greenland and Laurentide ice sheets interrupted by glacier advance during abrupt coolings. *Quaternary Science Reviews 229*, 106091, https://doi.org/10.1016/j.quascirev.2019.106091.
Young, N. E., Briner, J. P., Rood, D. H., Finkel, R. C., Corbett, L. B. & Bierman, P. R. 2013a: Age of the Fjord Stade moraines in the Disko Bugt region, western Greenland, and the 9.3 and 8.2 ka cooling events. *Quaternary Science Reviews 60*, 76–90.
Young, N. E., Lesnek, A. J., Cuzzone, J. K., Briner, J. P., Badgeley, J. A., Balter-Kennedy, A., Graham, B. L., Cluett, A., Lamp, J. L., Schwartz, R., Tuna, T., Bard, E., Caffee, M. W., Zimmerman, S. R. H. & Schaefer, J. M. 2021b: In situ cosmogenic ^{10}Be-^{14}C-^{26}Al measurements from recently deglaciated bedrock as a new tool to decipher changes in Greenland Ice Sheet size. *Climate of the Past 17*, 419–450.
Young, N. E., Schaefer, J. M., Briner, J. P. & Goehring, B. M. 2013b: A ^{10}Be production-rate calibration for the Arctic. *Journal of Quaternary Science 28*, 515–526.
Zech, R., Glaser, B., Sosin, P., Kubik, P. W. & Zech, W. 2005: Evidence for long-lasting landform surface instability on hummocky moraines in the Pamir Mountains (Tajikistan) from ^{10}Be surface exposure dating. *Earth and Planetary Science Letters 237*, 453–461.

Supporting Information

Additional Supporting Information to this article is available at http://www.boreas.dk.

Fig. S1. Map of NE Greenland including the locations discussed in the text and showing previously published ^{14}C (Håkansson 1974, 1975; Weidick 1977, 1996; Funder *et al*. 1978, 1990; Marienfeld *et al*. 1991; Landvik 1994; Wagner *et al*. 2000; Bennike & Björck 2002; Smith *et al*.

2023) and ^{10}Be ages (Håkansson *et al*. 2007, 2009, 2011; Kelly *et al*. 2008; Lowell *et al*. 2013; Levy *et al*. 2014, 2016; Larsen *et al*. 2018, 2022; Biette *et al*. 2020; Skov *et al*. 2020; Garcia-Oteyza *et al*. 2023; Roberts *et al*. 2024) concerning the deglaciation. In addition, the deglaciation information from two shelf marine sediment cores is provided (Davies *et al*. 2022; Pados-Dibattista *et al*. 2022). The geographical division (NE vs. central-east Greenland) follows that of the Geological Survey of Denmark and Greenland (Dawes & Glendal 2007).